



Lithofacies characterization and source rock assessment of the lower-middle Miocene Successions in the northern part of Ramadan oil field, central Gulf of Suez, Egypt

Mohamed M El Nady¹ · Fatma S. Ramadan² · Wafaa A. El Hemimey² · Ahmed H. Saleh²

Received: 27 April 2021 / Accepted: 23 February 2022 / Published online: 26 March 2022
© The Author(s) 2022

Abstract

Facies of rifting basins reflect different depositional environments from deep to shallow conditions. The present study focuses on subsurface facies characterization and source rock assessment of Kareem and Rudeis rocks in six wells lying in the central Gulf of Suez. The distribution of the lithologic patterns delineated through several constructed facies maps. Porosity cross-plots of Kareem and Rudeis formations to determine the rock minerals and porosity attitudes. Rock–Eval pyrolysis was applied to determine the kerogen type, organic matter richness, percentage, and maturation of the source rocks. The greater depth of the two formations was reflected in the western parts while their stratigraphic thickness increases toward the east and the north directions, with decreasing thickness towards the west direction due to an underlain basin structure of the pre-Miocene. Isolith maps show three deep marine lithologies for the two formations with the anhydrite as a fourth shallow marine lithology in the Kareem Formation only. These lithofacies reflect the turnover from the deep to the shallow depositional environment. The facies change from a main shaly limestone in the Rudeis Formation to calcareous shale in the Kareem formation, indicating transmutation from the lower Miocene deep to the middle Miocene shallow marine environments. The cross-plots reflected the existence of limestone, shale, and anhydrite. Geochemically, both formations are marginally good source rock with a marginally good generation of mixed type II/III and type III. Accordingly, Rudeis and Kareem formations could be good reservoirs rather than being potential source rocks in the central Gulf of Suez.

Keywords Miocene rocks · Source rock · Geochemical analysis · Rudeis and Kareem formations · Cross-plot

Introduction

The Lithofacies analysis explains the relationship between the sedimentary grains and the depositional environment conditions as well as the organofacies relevance to the amount and kind of organic materials in the depositional environment. Consequently, the non-marine source of hydrocarbon is completely different from that of deltaic and marine sources whether shale or carbonate source rock, and this is proved by several parameters that geochemically

illustrated. The successions of the Miocene in the central Gulf of Suez are shallow to open marine environments affected mainly by the structure framework developed through the Early-Middle Miocene time (Lashin and El Naby 2014). Organic-rich source rocks and good quality reservoir rocks found in the lower-middle Miocene sediments of Gharandal Group (Nukhul, Rudeis, and Kareem formations). These sediments are superimposed by the Ras Malaab Group (Belayim, South Gharib, Zeit formations) which, comprises mostly of evaporite, salt, and anhydrite deposits formed during the Middle-Upper Miocene and provide excellent regional cap rocks for Miocene reservoirs rocks from syn-rift periods (El Khadragy et al. 2016).

The organic abundance, kerogen category, and thermal progress in the Gulf of Suez were investigated to ascertain the probabilities of hydrocarbon generation by various authors, such as Mohamed et al. (2013) and Hadad et al. (2021). Five potential horizons of source rock through the Late Cretaceous–Miocene successions suggested by El

Responsible Editor: Santanu Banerjee

✉ Ahmed H. Saleh
Ahmohammed@zu.edu.eg

¹ Exploration Department, Egyptian Petroleum Research Institute, Cairo, Egypt

² Geology Department, Faculty of Science, Zagazig University, Zagazig, Egypt

Diasty and Peters (2014) based on Rock–Eval data and total organic carbon (TOC). The objectives of our work accomplished the following: (1) integrate the lithostratigraphic patterns by constructing isopach, depth, isolith, and lithofacies stratigraphic maps; (2) evaluate mineralogy, rock matrix, and porosity using binary and tri-porosity (M–N) cross-plot of the Rudeis and Kareem formations at the well R-5A; this is accomplished using neutron, sonic, and density logs as they are immediately affected by the matrix composition; and (3) use the obtainable geochemical data to define the kind of carbon-based matter, the organic enrichment, and establishing the thermal maturity of the source rocks.

Geologic setting

The Gulf of Suez rift basin has very substantial geologic characteristics due to its structural implication, Sedimentological environments, and hydrocarbon potentialities. The diversity of structural implications reflected the rift tectonics and lead to the establishment of the Gulf of Suez and the Red Sea (Shazly et al. 2013). According to geophysical and geological evidence, the central part of the Gulf of Suez exhibits many elongated, narrow depositional troughs. It is

cut by a complex system of faults that range from N-S to NNE-SSW, as well as E-W trending normal faults along the rift boundaries and within the rift basin and NE trending strike-slip faults that transverse the Gulf basin. The study area lies between longitudes $33^{\circ} 00'$ and $33^{\circ} 18'$ E and latitudes $28^{\circ} 40'$ and $28^{\circ} 50'$ N (Fig. 1). The Ramadan oil field is significant in the Gulf of Suez. It covers about 2850 acres (11.5 km^2) in the offshore, middle province of the Gulf of Suez basin, 174 km southeast from Suez City (El Shazly and Garossino 1991).

Three major tectonic rifting episodes caused the generation of a thick sedimentary succession in the Gulf of Suez rifting basin, which spans from the Paleozoic to the Cenozoic. These rifting episodes reflected three lithostratigraphic mega-sequences: a pre-rift (Paleozoic–Eocene) sequence, a syn-rift (Oligocene–Miocene) sequence, and a post-rift (Pliocene–Holocene) sequence (El-Ghali et al. 2013). The reservoirs of the Gulf of Suez span from Cambrian Nubian sandstone to the Miocene formations, with an individual field, reserve up to 1 million barrels from some oil/gas fields in the Gulf of Suez (Fig. 2). These successions vary in thickness, hydrocarbon potential, lithology, areal spreading, and sedimentation environment. The pre-Miocene sediments comprise Paleozoic to Lower Cretaceous Nubian

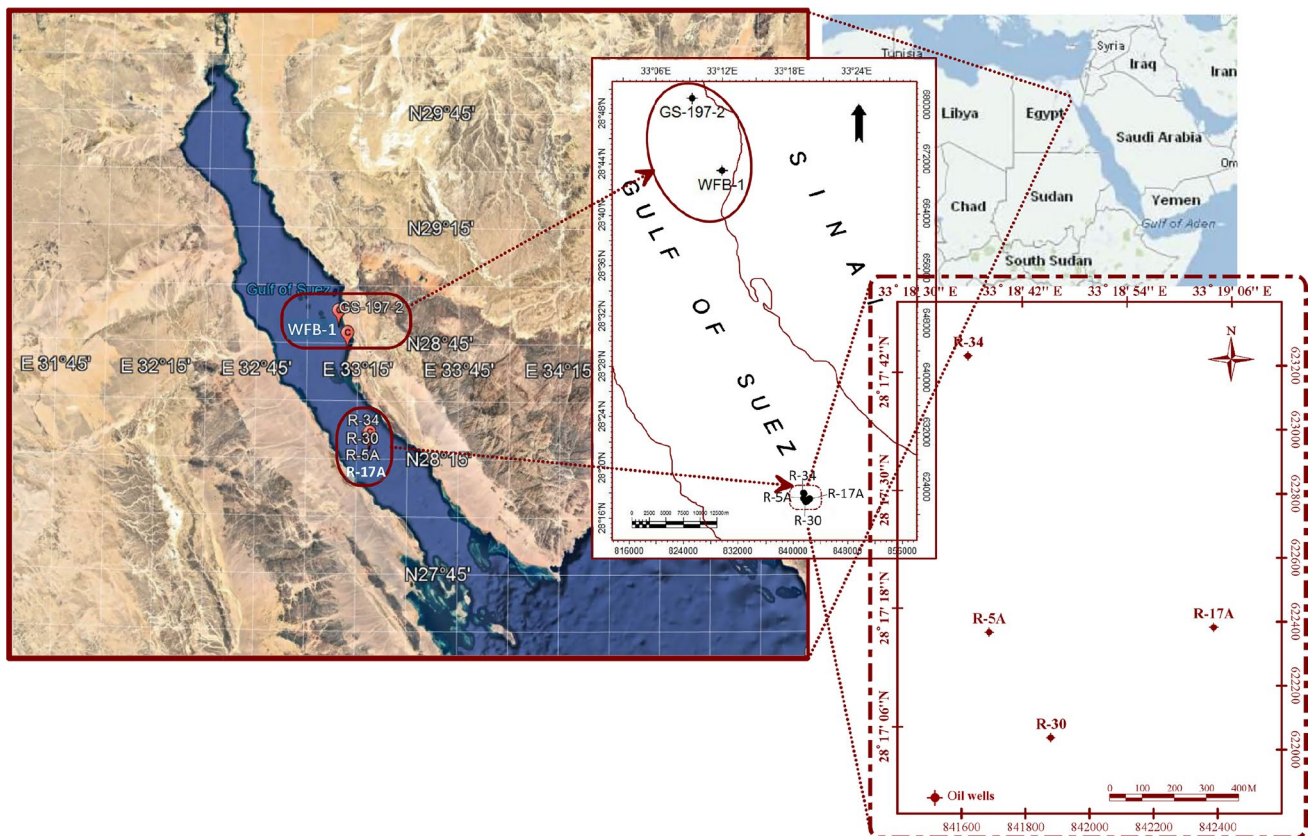


Fig. 1 Location map of the studied area, central Gulf of Suez, Egypt

sandstones capped by upper Cretaceous to Eocene carbonates and minor clastics. It is considered a petroleum-rich source rock due to the existence of the organic matter in carbonate and clastics sedimentary rocks. The carboniferous Ataqa group (Abu Durba and Rod El Hamal formations) consider good sources furnish the uppermost hydrocarbon reservoirs. The two major lithologic units represented in the overlying Miocene sediments are clastic sequences overlain by a series of evaporites where many reservoirs are considerable in the pre-Miocene sediments. The majority of the oil in the Gulf of Suez comes from the Miocene clastics unit which provides both source rocks and pays horizons, while the middle of Miocene evaporites deposits ensure a respectable seal for the traps developed through rifting juncture (Radwan 2020). Several potential source rocks are alternating from upper Cretaceous to Miocene (El Diasty et al. 2014). Numerous source rock suggestions fit the complex geological setting of the Gulf of Suez rift region, in which sediments are subjected to diverse geological circumstances which affected depositional environments through facies and lithology variations, propagation in the deepness of burying, and the organic matter richness. The Gulf of Suez is segregated with two accommodation zones (Zaafarana and Morgan accommodation zones) into three massive hydrocarbon territories with the alternating polarity of strata dip direction. The three territories arranged from north to south are Darag, Belayim, and Zeit territories. The central one (Belayim territory) where the area of study lies, is the most productive hydrocarbon province in Egypt (Fig. 3). It provides a promising future oil exploration in this region (Van Dijk et al. 2020).

Hughes et al. (1992) categorized the Rudeis Formation to differentiated lower and upper sedimentation behavior, with a borderline that coincides with the mid-Clysmic tectonic event, which is frequently visible in borehole gamma-ray logs. Moreover, the Mheiherrat, the Hawara, the Asl, and the Mreir are another Members segmentation of the Rudeis formation ranked by Schütz (1994). Its thickness and composition are variable due to sedimentation processes in a rapidly subsiding fault-controlled basin, as a clear thickness variation of the Rudeis Formation is reflected through the wells understudy. It consists mainly of sandy shales and calcareous shales with Globigerina shales and marls occurring choppy (Nabawy et al. 2019). Containing deep-water foraminifera and Globigerina marls and shales of the basal facies, the Rudeis Formation reflects an open marine depositional environment as it is considered the richest oil source rocks, deposited under the most favorable structural conditions (Makky et al. 2010 and Sallama et al. 2019).

The Kareem Formation is segmented by EGPC (1964) into Markha Member (Rahmi Member) and the overlying Shagar Member. Furthermore, the foraminifera biostratigraphically dates the Kareem Formation as a Middle

Miocene age. The Shagar Member is represented by fossiliferous shales, marls, limestone intercalations, and minor sandstone. Through the beginning of Langhian time, a regional marine regression along the Gulf of Suez lead to the deposition of a thin anhydrite bed at the Rahmi member with an oscillating presence due to lateral facies changes (Radwan and Sen 2020). The Kareem and the Rudeis formations were recorded on the rift shoulders and north in the current gulf's tip. It is also worth mentioning that the two formations show excellent sand reservoirs with porosities ranging from 11 to 24%, showing or even producing oil from many fields. As reservoirs, The Rudeis and Kareem formations limestone and sandstone reserve about 20% and 23%, respectively, of production potential in the Gulf of Suez.

Materials and methods

The thickness changes and depth distribution for different successions and facies have a main role in petroleum source rock and reservoir rock assessment. The wells data used in this study are the composites and normal electric logs of gamma-ray, sonic, deep resistivity logs for the Rudeis and the Kareem formations in four wells (R-34, R-17A, R-5A, R-30), with the neutron and density logs, run in R-5A well only. The geochemical report of the Rudeis and the Kareem formations in WFB-1 and GS197-2 wells for the geochemical analysis for the sediments of the two formations as source rocks in these wells. Through our work on the lower-middle Miocene sediments in the north of Ramadan oil field, the Rudeis and the Kareem formations were lithologically and geochemically analyzed using these data. Correlation cross section (chart), relief maps, isopach maps, isolith maps, and lithofacies maps made for the studied rock units, using the technique of Krumbein and Sloss (1963). A directed NW–SE stratigraphic correlation chart reflecting the differences in the formations depths, thickness, and the laterally changed facies either by sedimentation or structural effect also illustrates the increasing and decreasing in certain types of rocks like shales, limestone, and sandstone percent's which in turn leads to clear identification for the different depositional environments of the source and reservoir rocks. The stratigraphic correlation chart helps in locating the proposed structural lineaments and features positions and attitudes like faults and folds. It will lead to constructing the structural setting of the area under study that affects the syn-rift sedimentation circumstances which guided us to the correct interpretations for the depth change behavior through the relief map, the thickness propagation through the isopach maps, and the presences of the different facies and lithologies in the under investigation through the isolith and facies maps (Table 1).

Table 1 Thicknesses and ratios for the facies of Rudeis and Kareem formations

| Well name | Formation | Depth (ft) | Total thickness (ft) | Shale thickness (ft) | Limestone thickness (ft) | Marl thickness (ft) | Sand thickness (ft) | Anhydrite thickness (ft) | Clastic ratio | Sand/shale ratio |
|-----------|-----------|------------|----------------------|----------------------|--------------------------|---------------------|---------------------|--------------------------|---------------|------------------|
| R-34 | Kareem | –7064 | 493 | 180 | 115 | 170 | 0 | 28 | 2.45 | 0 |
| R-17A | | –7134 | 430 | 145 | 110 | 135 | 0 | 40 | 1.87 | 0 |
| R-5A | | –7411 | 379 | 200 | 144 | 0 | 5 | 30 | 1.18 | 0.03 |
| R-30 | | –7198 | 362 | 114 | 224 | 0 | 0 | 24 | 0.46 | 0 |
| R-34 | Rudeis | –7557 | 1796 | 491 | 910 | 395 | 0 | 0 | 0.97 | 0 |
| R-17A | | –7564 | 2020 | 785 | 680 | 555 | 0 | 0 | 1.97 | 0 |
| R-5A | | –7790 | 1638 | 500 | 725 | 413 | 0 | 0 | 1.26 | 0 |
| R-30 | | –7560 | 1858 | 820 | 1038 | 0 | 0 | 0 | 0.79 | 0 |

Using thin sections, we can directly differentiate between all lithologies as a reservoir evaluation substantial step (Dott 1964). Moreover, we can use well logging relations and cross-plots indirectly as a lithology determination method. Applying porosity logs data, the binary and tri-porosity (M–N) cross-plots for the two formations in the R-5A well were accomplished using Schlumberger charts (2009) for rock type and mineral composition identification. The different rock minerals can be distinguished using the three porosity logs (neutron, density, and sonic) cross-plotted with each other as it is influenced by matrix components. It is easy to limit the porosity and assess the matrix characteristics of the Formation encountered from the reading of two or three porosity logs.

Furthermore, all ninety cutting samples of the previously mentioned formations in WFB-1 and GS197-2 wells scheduled the highest and lowest values for every 10 consecutive samples (Table 2). This work focuses on quantitative and qualitative analyses, as the interpretation of the source rock. Quantitative analysis determines the total organic carbon (TOC). Qualitative analysis identifies the nature of the organic matter from Rock–Eval pyrolysis and the percentages of organic matter present in the kerogen of the source rocks (Rudeis and Kareem formations). The stage of maturation of organic matter is detected by the calculated vitrinite reflectance (R0%) as it is the most commonly used method (Waples 1985), and Rock–Eval pyrolysis data as Tmax and production index (PI) for Lower Miocene rock units occurred in the area around the studied wells, at the central part of the Gulf of Suez.

Thirty-one samples represented the Rudeis Formation, which consists of shale, sandstone, and trace limestone were analyzed from the GS197-2 well (Table 3). Fifty-nine samples were analyzed from the Rudeis and Kareem formations from the WFB-1 well composed of 33 samples for the Rudeis Formation and 26 samples for Kareem Formation, which consists of shale, sandstone, and subordinate limestone (Table 4). The results are represented by various

parameters such as total organic carbon (TOC %) describes the quantity of organic carbon in a rock sample and includes both kerogen and bitumen (Hunt 1996). Using LECO SC-632, the crushed rock samples geochemically analyzed to determine TOC content. About 0.2 g of the sample is carefully weighed and placed in a ceramic crucible and then treated with 10% concentrated hydrochloric acid to remove carbonates, washed with distilled water more times, dried, combusted with pure oxygen in a LECO SC-632 carbon analyzer at about 1450 centigrade. Carbon dioxide (CO₂) created by the combustion of organic matter in the sample is quantitatively measured utilizing an infrared detector. The pyrolysis analyses have been achieved by applying the Rock–Eval Pyrolysis technique (Espitalié et al. 1977) for the samples that have a TOC % more than 0.5. Pyrolysis results were represented by different parameters such as the contents of volatile hydrocarbons (S₁ peak) liberated at temperatures less than 300 °C and pyrolytic hydrocarbons (S₂ peak) liberated throughout the temperature-programmed pyrolysis at temperatures ranging from 300 to 600 °C (Espitalié et al. 1985). The S₁ and S₂ peaks are articulated in milligrams of hydrocarbons per gram of rock (mg/g) and S₃ peak symbolizes the amount of CO₂ created by pyrolysis of the organic matter and is uttered in CO₂ in mg/rock in g (mg/g). All these parameters are applied in the current investigation to calculate the hydrogen index (HI = mg HC/g TOC) and oxygen index (OI = mg CO₂/g TOC); generating potential (GP) is the summation of S₁ and S₂, and type of hydrocarbons products (QI = S₂/S₃) (Behar et al. 2001; Carvajal-Ortiz and Gentz 2015).

Results and discussion

Miocene facies (lower-middle)

The syn rifting sediments characterized by different thicknesses for the same horizon as the sedimentary succession of

Table 2 Pyrolysis data of the Lower Miocene source rocks; Rudeis and Kareem formations in WFB-1 well and Rudeis Formation in GS197-2 well, Central Gulf of Suez, Egypt

| Well name | Fm | Depth (ft) | TOC (%) | S ₁ (Mg/g) | S ₂ (Mg/g) | T _{max} (°C) | HI (Mg/g) | OI (Mg/g) | PI | QI | GP | Ro |
|-----------|--------|------------|-------------------|-----------------------|-----------------------|-----------------------|-----------------|-----------------|----------------|---------|---------|---------|
| WFB-1 | Rudeis | 781–806 | 0.39–1.21 (0.75) | 0.14–0.29 (0.197) | 1.14–3.16 (2.08) | 421–431 (429.3) | 213–762 (303.1) | 153–495 (260.5) | 0.1–0.2 (0.11) | 0.7–1.7 | 1.3–3.4 | 0.4–0.6 |
| | | 809–839 | 0.56–1.09 (0.75) | 0.17–0.32 (0.24) | 0.82–2.05 (1.36) | 426–430 (428.3) | 146–240 (182) | 142–317 (227) | 0.1–0.2 (0.15) | 0.6–1.1 | 1.0–2.4 | 0.5–0.6 |
| | | 842–906 | 0.33–0.66 (0.41) | 0.13–0.35 (0.21) | 0.07–0.95 (0.57) | 421–433 (427.6) | 19–203 (139.3) | 58–282 (134.1) | 0.2–0.7 (0.32) | 0.2–3.1 | 0.2–1.2 | 0.8 |
| Kareem | | 708–733 | 0.8–1.19 (1.03) | 0.16–0.24 (0.21) | 2.04–3.7 (2.94) | 425–431 (427.2) | 253–343 (285.1) | 117–271 (108.4) | 0.0–0.1 (0.1) | 0.9–2.3 | 2.2–3.9 | 0.4–0.6 |
| | | 736–761 | 0.48–1.13 (0.83) | 0.17–0.24 (0.20) | 0.93–3.74 (2.1) | 425–432 (427.6) | 192–331 (248.7) | 150–325 (225) | 0.1–0.2 (0.11) | 0.7–2.2 | 1.1–3.9 | 0.5–0.6 |
| | | 764–778 | 0.44–0.99 (0.75) | 0.16–0.35 (0.23) | 0.77–2.16 (1.8) | 421–430 (425.6) | 148–291 (238.1) | 185–268 (216.2) | 0.1–0.2 (0.13) | 0.7–1.5 | 1.0–3.0 | 0.4–0.5 |
| GS197-2 | Rudeis | 799–841 | 0.80–1.23 (0.955) | 0.15–0.32 (0.228) | 1.05–2.43 (1.705) | 428–433 (430.2) | 114–241 (178.6) | 200–371 (261.9) | 0.1–0.2 (0.11) | 0.3–1.2 | 1.5–2.7 | 0.5–0.6 |
| | | 846–888 | 0.81–1.06 (0.953) | 0.2–0.36 (0.253) | 1.2–3.03 (2.0) | 429–434 (431.3) | 148–303 (212.5) | 193–394 (256) | 0.0–0.1 (0.1) | 0.4–1.6 | 1.4–3.4 | 0.6–0.7 |
| | | 892–939 | 0.42–1.17 (0.923) | 0.22–0.41 (0.291) | 0.56–3.2 (2.0) | 419–435 (430.7) | 133–274 (209.8) | 169–757 (317.7) | 0.1–0.3 (0.14) | 0.2–1.5 | 0.8–3.6 | 0.4–0.7 |

TOC, total organic carbon (weight percentage of the whole rock); S₁, low hydrocarbon yield (mg hydrocarbon/g rock); S₂, high hydrocarbon yield (mg hydrocarbon/gm rock); HI, hydrogen index (mg hydrocarbon/gm TOC); OI, oxygen index (mg CO₂/gm TOC); Tmax, temperature at which maximum emission of high temperature (S₂) hydrocarbon occurs (°C); PI, production index (S₁/S₁ + S₂); GP, generation potential (S₁ + S₂)

the rift basins represent a rapidly changed sedimentation rate affected by the structural deformation, which affects the sedimentation process. A stratigraphic correlation cross section (chart) was constructed using four of the studied wells (R-34, R-17A, R-5A, R-30 wells) directed NW–SE to explain the depth, thickness, and sedimentological environments of the Miocene successions. It reflects the presence of the Rudeis and the Kareem formations in the study area without any missing with slightly different depth and thickness. It shows that the Miocene shale and marl represent a perfect example of the source rock rich in organic matter as the Rudeis Globigerina marls and shales. The fossils were recorded as many different species at different depths (Fig. 4). It shows different sediments in the same capricious depositional environments where the Rudeis sediments are latterly changed from mainly fossiliferous limestone in the northwestern parts (R1-34 well) to mainly globigerina marl and shales as reflected from the electric logs (gamma-ray log) which reflected high shale content in the southeastern parts. This indicated deeper sedimentation water in the southern parts than the northern parts for Rudeis Formation. On the other hand, the lower part of Kareem formation reflected a shallow (lagoon) environment due to the major regional marine regression along the Gulf of Suez which resulted in the deposition of a thin anhydrite layer at the Rahmi member. This thin anhydrite bed is well represented through the understudy wells on the section nearly with the same thickness (Fig. 4). Fossiliferous shales, marls, and intermittent limestone thin beds represent the Shagar Member. The Kareem formation has more shale southward the same as the Rudeis Formation which reflects deep water of deposition in well R5-30 with an oscillating presence because of the laterally changed facies (Radwan and Sen 2020).

The deepness and surfaces distribution of the Miocene sedimentary formations are reflected through structure contour maps or depth maps (relief maps) as the depth of organic matter burial is an important agent for Creating a suitable thermal and non-oxygen (anoxic) environment for oil maturation and generation. The relief maps of the Rudeis and the Kareem formations show an increased depth in the western parts of the study area around the R-5A well where it recorded a maximum depth of 7411 ft. for Rudeis Formation and 7790 ft. for Kareem formation, respectively (Fig. 5a, b). This means a suitable thermal and non-oxygen environment for oil maturation and generation in western parts of the investigated area. The depth decreases towards the northern, eastern, and southeastern parts of the study area where it recoded a minimum depth of 7557 ft. for the Rudeis Formation and 7064 ft. with respect to the Kareem Formation of the R-34 well. This reflects a sedimentary basin with a western thicker interval (basin depocenter) and northern, northwestern, and western thinner low dip gradient platform margin for the Rudeis formation which inverted

Table 3 Results of TOC and Rock–Eval pyrolysis of Rudeis Formation in GS197-2 well, Central Gulf of Suez, Egypt

| Well | Fm. name | Depth (ft) | TOC wt% | S ₁ (mg/g) | S ₂ (mg/g) | S ₃ (mg/g) | T _{max} | HI | OI | QI | PI | GP | RO |
|--------------|-----------|------------|---------|-----------------------|-----------------------|-----------------------|------------------|-----|-----|-----|-----|-----|-----|
| GS197-2 well | Rudeis Fm | 799 | 1.04 | 0.32 | 2.21 | 2.67 | 431 | 213 | 257 | 0.8 | 0.1 | 2.5 | 0.6 |
| | | 804 | 1.23 | 0.21 | 1.71 | 2.51 | 431 | 139 | 204 | 0.7 | 0.1 | 1.9 | 0.6 |
| | | 809 | 1.01 | 0.25 | 2.43 | 2.02 | 433 | 241 | 200 | 1.2 | 0.1 | 2.7 | 0.6 |
| | | 813 | 0.86 | 0.18 | 1.36 | 2.16 | 428 | 158 | 251 | 0.6 | 0.1 | 1.5 | 0.5 |
| | | 818 | 0.91 | 0.16 | 1.51 | 1.91 | 430 | 166 | 210 | 0.8 | 0.1 | 1.7 | 0.5 |
| | | 823 | 0.92 | 0.15 | 1.05 | 3.41 | 431 | 114 | 371 | 0.3 | 0.1 | 1.2 | 0.6 |
| | | 827 | 0.92 | 0.28 | 1.72 | 2.2 | 430 | 187 | 239 | 0.8 | 0.1 | 2 | 0.6 |
| | | 832 | 0.8 | 0.29 | 1.56 | 2.39 | 430 | 195 | 299 | 0.7 | 0.2 | 1.9 | 0.6 |
| | | 837 | 0.88 | 0.18 | 1.28 | 3 | 428 | 146 | 341 | 0.4 | 0.1 | 1.5 | 0.5 |
| | | 841 | 0.98 | 0.26 | 2.22 | 2.42 | 430 | 227 | 247 | 0.9 | 0.1 | 2.5 | 0.6 |
| | | 846 | 0.96 | 0.2 | 2.07 | 2.23 | 432 | 216 | 232 | 0.9 | 0.1 | 2.3 | 0.6 |
| | | 850 | 0.91 | 0.2 | 1.71 | 2.7 | 429 | 188 | 297 | 0.6 | 0.1 | 1.9 | 0.6 |
| | | 855 | 1 | 0.24 | 1.92 | 2.41 | 431 | 192 | 241 | 0.8 | 0.1 | 2.2 | 0.6 |
| | | 860 | 0.81 | 0.2 | 1.2 | 3.19 | 431 | 148 | 394 | 0.4 | 0.1 | 1.4 | 0.6 |
| | | 864 | 1.06 | 0.25 | 1.8 | 3.08 | 432 | 170 | 291 | 0.6 | 0.1 | 2 | 0.6 |
| | | 869 | 0.98 | 0.28 | 2.29 | 2.06 | 433 | 234 | 210 | 1.1 | 0.1 | 2.6 | 0.6 |
| | | 874 | 1.01 | 0.2 | 1.79 | 2.45 | 434 | 177 | 243 | 0.7 | 0.1 | 2 | 0.7 |
| | | 878 | 0.97 | 0.33 | 2.36 | 2.16 | 431 | 243 | 223 | 1.1 | 0.1 | 2.7 | 0.6 |
| | | 883 | 0.83 | 0.27 | 2.11 | 1.96 | 429 | 254 | 236 | 1.1 | 0.1 | 2.4 | 0.6 |
| | | 888 | 1 | 0.36 | 3.03 | 1.93 | 432 | 303 | 193 | 1.6 | 0.1 | 3.4 | 0.6 |
| | | 892 | 0.98 | 0.26 | 2.57 | 1.66 | 432 | 262 | 169 | 1.5 | 0.1 | 2.8 | 0.6 |
| | | 897 | 0.84 | 0.28 | 1.93 | 2.33 | 429 | 230 | 277 | 0.8 | 0.1 | 2.2 | 0.6 |
| | | 902 | 1.08 | 0.28 | 2.74 | 1.84 | 432 | 254 | 170 | 1.5 | 0.1 | 3 | 0.6 |
| | | 906 | 1 | 0.28 | 2.08 | 2.15 | 434 | 208 | 215 | 1 | 0.1 | 2.4 | 0.7 |
| | | 911 | 1.2 | 0.28 | 2.4 | 2.47 | 432 | 200 | 206 | 1 | 0.1 | 2.7 | 0.6 |
| | | 916 | 0.94 | 0.22 | 1.65 | 3.5 | 433 | 176 | 372 | 0.5 | 0.1 | 1.9 | 0.6 |
| | | 920 | 1.17 | 0.41 | 3.2 | 2.2 | 433 | 274 | 188 | 1.5 | 0.1 | 3.6 | 0.6 |
| | | 925 | 1.01 | 0.37 | 1.96 | 3.63 | 432 | 194 | 359 | 0.5 | 0.2 | 2.3 | 0.6 |
| | | 930 | 0.85 | 0.23 | 1.87 | 2.66 | 435 | 220 | 313 | 0.7 | 0.1 | 2.1 | 0.7 |
| | | 934 | 0.67 | 0.33 | 1.05 | 3.14 | 427 | 157 | 469 | 0.3 | 0.2 | 1.4 | 0.5 |
| | | 939 | 0.42 | 0.27 | 0.56 | 3.18 | 419 | 133 | 757 | 0.2 | 0.3 | 0.8 | 0.4 |

TOC, total organic carbon, wt. %; S₁, free hydrocarbons content, mg HC/g rock; S₂, remaining hydrocarbons generative potential, mg HC/g rock; S₃, carbon dioxide yield, mg CO₂/g rock; HI, hydrogen index = S₂ × 100/TOC, mg HC/TOC; OI, oxygen index = S₃ × 100/ TOC, mg CO₂/g TOC; T_{max} = temperature at maximum of S₂ peak; PI, production index = S₁/(S₁ + S₂); calculated Ro = vitrinite reflectance measurement = ((0.018 × T_{max}) - 7.16)

slightly into high dip gradient for the Kareem Formation. The Rudeis Formation isopach map shows an increasing thickness toward the eastern part of the study area, where it reaches the maximum thickness of 2020 ft. at the southeastern part around the R-17 well. It decreases towards the west reaching the minimum thickness of 1638 ft. in the R-5A well (Fig. 6a). The isopach map of the Kareem Formation shows an increased thickness towards the northern part of the study area, recording the maximum thickness of 493 ft. in the R-34 well. The thickness decreases towards the south reaching a minimum thickness of about 362 ft. in the R-30 well (Fig. 6b). The largest volume of the source rock is indicated the volume of kerogen able to produce oil and gas.

Shale isolith map of the Rudeis Formation illustrates that the shale thickness decreases towards the northwest direction as it reaches the minimum value of 491 ft. in the R-34 well compared to a gradual increase to maxima of ca. 870 ft. towards the R-30 well (Fig. 7a). The marl isolith map illustrates that the marl thickness decreases towards the south as it reaches a minimum value of 40 ft. within the R-30 well. The thickness increases towards the northeast with a maximum value of 555 ft. in the R-17A well (Fig. 7b). The limestone isolith map illustrates that the limestone thickness decreases towards the northeast until it reaches a minimum value of 680 ft. around the R-17A well (Fig. 7c). It increases towards the south, reaching a maximum value of 1038 ft. around the R-30 well. The anhydrite

Table 4 Results of TOC and Rock–Eval pyrolysis of Kareem and Rudeis formations in WFB-1 well, Central Gulf of Suez, Egypt

| Well | Fm. name | Depth (ft) | TOC (wt%) | S1 (mg/g) | S2 (mg/g) | S3 (mg/g) | Tmax | HI | OI | QI | PI | GP | RO | | |
|------------|-----------|------------|-----------|-----------|-----------|-----------|------|------|-----|-----|-----|-----|-----|-----|-----|
| WFB-1 well | Kareem Fm | 708 | 1.01 | 0.22 | 3.2 | 1.65 | 425 | 317 | 163 | 1.9 | 0.1 | 3.4 | 0.4 | | |
| | | 711 | 1.12 | 0.24 | 3.05 | 1.74 | 427 | 272 | 155 | 1.8 | 0.1 | 3.3 | 0.5 | | |
| | | 714 | 1.19 | 0.23 | 3.16 | 1.39 | 426 | 266 | 117 | 2.3 | 0.1 | 3.4 | 0.5 | | |
| | | 717 | 0.93 | 0.23 | 2.43 | 1.97 | 425 | 261 | 212 | 1.2 | 0.1 | 2.7 | 0.5 | | |
| | | 719 | 0.8 | 0.17 | 2.04 | 2.17 | 427 | 255 | 271 | 0.9 | 0.1 | 2.2 | 0.5 | | |
| | | 722 | 0.95 | 0.17 | 2.4 | 1.62 | 430 | 253 | 171 | 1.5 | 0.1 | 2.6 | 0.6 | | |
| | | 725 | 1.01 | 0.21 | 2.92 | 2.01 | 426 | 289 | 199 | 1.5 | 0.1 | 3.1 | 0.5 | | |
| | | 728 | 1.1 | 0.23 | 3.64 | 1.83 | 428 | 331 | 166 | 2 | 0.1 | 3.9 | 0.5 | | |
| | | 731 | 1.08 | 0.16 | 2.85 | 1.9 | 431 | 264 | 176 | 1.5 | 0.1 | 3 | 0.6 | | |
| | | 733 | 1.08 | 0.24 | 3.7 | 1.88 | 427 | 343 | 174 | 2 | 0.1 | 3.9 | 0.5 | | |
| | | 736 | 0.96 | 0.22 | 2.78 | 2.19 | 429 | 290 | 228 | 1.3 | 0.1 | 3 | 0.6 | | |
| | | 739 | 0.97 | 0.2 | 2.07 | 2.45 | 426 | 213 | 253 | 0.8 | 0.1 | 2.3 | 0.5 | | |
| | | 742 | 0.83 | 0.24 | 1.68 | 2.53 | 427 | 202 | 305 | 0.7 | 0.1 | 1.9 | 0.5 | | |
| | | 745 | 0.64 | 0.19 | 1.6 | 1.41 | 429 | 250 | 220 | 1.1 | 0.1 | 1.8 | 0.5 | | |
| | | 747 | 0.97 | 0.17 | 1.86 | 1.5 | 432 | 192 | 155 | 1.2 | 0.1 | 2 | 0.6 | | |
| | | 750 | 1.03 | 0.18 | 2.23 | 2.13 | 427 | 217 | 207 | 1 | 0.1 | 2.4 | 0.5 | | |
| | | 753 | 0.8 | 0.2 | 2.35 | 2.6 | 426 | 294 | 325 | 0.9 | 0.1 | 2.6 | 0.5 | | |
| | | 756 | 1.13 | 0.2 | 3.74 | 1.7 | 427 | 331 | 150 | 2.2 | 0.1 | 3.9 | 0.5 | | |
| | | 758 | 0.5 | 0.21 | 1.52 | 1.07 | 425 | 304 | 214 | 1.4 | 0.1 | 1.7 | 0.5 | | |
| | | 761 | 0.48 | 0.18 | 0.93 | 0.92 | 428 | 194 | 192 | 1 | 0.2 | 1.1 | 0.5 | | |
| | | 764 | 0.82 | 0.18 | 1.92 | 1.94 | 428 | 234 | 237 | 1 | 0.1 | 2.1 | 0.5 | | |
| | | 767 | 0.89 | 0.16 | 2.16 | 1.65 | 428 | 243 | 185 | 1.3 | 0.1 | 2.3 | 0.5 | | |
| | | 770 | 0.81 | 0.2 | 1.95 | 1.72 | 430 | 241 | 212 | 1.1 | 0.1 | 2.2 | 0.6 | | |
| | | 772 | 0.99 | 0.28 | 2.69 | 1.85 | 425 | 272 | 187 | 1.5 | 0.1 | 3 | 0.5 | | |
| | | 775 | 0.52 | 0.21 | 0.77 | 1.08 | 422 | 148 | 208 | 0.7 | 0.2 | 1 | 0.4 | | |
| | | 778 | 0.44 | 0.35 | 1.28 | 1.18 | 421 | 291 | 268 | 1.1 | 0.2 | 1.6 | 0.4 | | |
| | | Rudeis Fm | Rudeis Fm | 781 | 0.88 | 0.16 | 2.2 | 1.39 | 431 | 250 | 158 | 1.6 | 0.1 | 2.4 | 0.6 |
| | | | | 784 | 0.86 | 0.16 | 1.97 | 1.72 | 431 | 229 | 200 | 1.1 | 0.1 | 2.1 | 0.6 |
| | | | | 786 | 0.82 | 0.18 | 2.08 | 1.76 | 431 | 254 | 215 | 1.2 | 0.1 | 2.3 | 0.6 |
| | | | | 789 | 0.57 | 0.22 | 1.52 | 1.94 | 430 | 267 | 340 | 0.8 | 0.1 | 1.7 | 0.6 |
| | | | | 791 | 0.5 | 0.14 | 1.14 | 1.07 | 421 | 228 | 214 | 1.1 | 0.1 | 1.3 | 0.4 |
| | | | | 794 | 1.21 | 0.18 | 2.74 | 1.85 | 431 | 226 | 153 | 1.5 | 0.1 | 2.9 | 0.6 |
| | | | | 798 | 1.04 | 0.2 | 3.16 | 1.84 | 431 | 304 | 177 | 1.7 | 0.1 | 3.4 | 0.6 |
| | | | | 800 | 0.39 | 0.29 | 2.97 | 1.93 | 430 | 762 | 495 | 1.5 | 0.1 | 3.3 | 0.6 |
| | | | | 803 | 0.77 | 0.17 | 1.64 | 1.68 | 430 | 213 | 218 | 1 | 0.1 | 1.8 | 0.6 |
| | | | | 806 | 0.43 | 0.27 | 1.28 | 1.87 | 427 | 298 | 435 | 0.7 | 0.2 | 1.6 | 0.5 |
| 809 | 0.73 | | | 0.2 | 1.75 | 1.68 | 430 | 240 | 230 | 1 | 0.1 | 2 | 0.6 | | |
| 811 | 0.67 | | | 0.17 | 1.32 | 1.78 | 429 | 197 | 266 | 0.7 | 0.1 | 1.5 | 0.6 | | |
| 814 | 0.68 | | | 0.18 | 1.16 | 1.86 | 429 | 171 | 274 | 0.6 | 0.1 | 1.3 | 0.6 | | |
| 817 | 0.68 | | | 0.21 | 1.37 | 1.77 | 427 | 202 | 260 | 0.8 | 0.1 | 1.6 | 0.5 | | |
| 822 | 0.91 | | | 0.3 | 2.05 | 2.88 | 427 | 225 | 317 | 0.7 | 0.1 | 2.4 | 0.5 | | |
| 825 | 1.09 | | | 0.32 | 1.6 | 2.08 | 429 | 147 | 191 | 0.8 | 0.2 | 1.9 | 0.6 | | |
| 828 | 0.92 | | | 0.2 | 1.45 | 1.31 | 430 | 158 | 142 | 1.1 | 0.1 | 1.7 | 0.6 | | |
| 830 | 0.7 | | | 0.28 | 1.04 | 1.28 | 428 | 149 | 183 | 0.8 | 0.2 | 1.3 | 0.5 | | |
| 833 | 0.72 | | | 0.32 | 1.58 | 1.72 | 429 | 219 | 239 | 0.9 | 0.2 | 1.9 | 0.6 | | |
| 836 | 0.57 | | | 0.22 | 0.84 | 1.1 | 427 | 147 | 193 | 0.8 | 0.2 | 1.1 | 0.5 | | |
| 839 | 0.56 | 0.22 | 0.82 | 1.13 | 426 | 146 | 202 | 0.7 | 0.2 | 1 | 0.5 | | | | |
| 842 | 0.66 | 0.22 | 0.95 | 0.7 | 427 | 144 | 106 | 1.4 | 0.2 | 1.2 | 0.5 | | | | |
| 845 | 0.32 | 0.14 | 0.26 | 0.66 | 425 | 81 | 206 | 0.4 | 0.4 | 0.4 | 0.5 | | | | |
| 848 | 0.35 | 0.21 | 0.63 | 0.41 | 421 | 180 | 117 | 1.5 | 0.3 | 0.8 | 0.4 | | | | |

Table 4 (continued)

| Well | Fm. name | Depth (ft) | TOC (wt%) | S1 (mg/g) | S2 (mg/g) | S3 (mg/g) | Tmax | HI | OI | QI | PI | GP | RO |
|------|----------|------------|-----------|-----------|-----------|-----------|------|-----|-----|-----|-----|-----|-----|
| | | 851 | 0.48 | 0.21 | 0.57 | 0.58 | 428 | 119 | 121 | 1 | 0.3 | 0.8 | 0.5 |
| | | 864 | 0.33 | 0.16 | 0.4 | 0.93 | 425 | 121 | 282 | 0.4 | 0.3 | 0.6 | 0.5 |
| | | 878 | 0.49 | 0.29 | 0.77 | 0.71 | 425 | 157 | 145 | 1.1 | 0.3 | 1.1 | 0.5 |
| | | 881 | 0.51 | 0.27 | 0.93 | 0.8 | 426 | 182 | 157 | 1.2 | 0.2 | 1.2 | 0.5 |
| | | 884 | 0.33 | 0.16 | 0.58 | 0.19 | 431 | 176 | 58 | 3.1 | 0.2 | 0.7 | 0.6 |
| | | 890 | 0.36 | 0.23 | 0.57 | 0.32 | 428 | 158 | 89 | 1.8 | 0.3 | 0.8 | 0.5 |
| | | 892 | 0.34 | 0.2 | 0.45 | 0.36 | 429 | 132 | 106 | 1.3 | 0.3 | 0.7 | 0.6 |
| | | 903 | 0.34 | 0.35 | 0.69 | 0.38 | 433 | 203 | 112 | 1.8 | 0.3 | 1 | 0.6 |
| | | 906 | 0.37 | 0.13 | 0.07 | 0.41 | 433 | 19 | 111 | 0.2 | 0.7 | 0.2 | 0.6 |

isolith map of the Kareem Formation (Fig. 8a) illustrates that the anhydrite thickness decreases in the direction of the south and southwest, recording 24 ft. in the R-30 well. It increases towards the east with a maximum value of 40 ft. around the R-17A well. The limestone isolith map (Fig. 8b) illustrates that the limestone thickness decreases towards the east as it reaches a minimum value of 110 ft. in the R-17A well. The thickness increases towards the south and reaches a maximum thickness of 224 ft. in the R-30 well. The marl isolith map (Fig. 8c) shows that the marl thickness decreases towards the south and southwest as it vanishes in the R-5A and R-30 wells. It increases towards the north and northeast and reaches a maximum value of 170 ft. in the R-34 well. The shale isolith map of the Kareem Formation (Fig. 8d) illustrates that shale thickness decreases towards the south and southeast until it reaches a minimum value of 114 ft. at the R-30 well. It increases towards the north and northwest with a maximum value of 200 ft. in the R-5A well (Radwan 2020). Through Fig. 9a, the lithofacies distribution map of the Rudeis Formation reveals that the sediments are composed chiefly of shaly limestone and calcareous shale displaying deep marine circumstances (Lashin and El-Naby 2014). The lithofacies distribution map of the Kareem Formation shows that the sediments are mainly composed of limestone and shaly limestone, indicating shallow to deep marine sedimentations settings as shown in (Fig. 9b).

Matrix analysis

Cross-plots are a convenient way to demonstrate how various combinations of logs respond to lithology and porosity, where the facies maps introduce a detailed lithological study (El Khadragey et al. 2016). The matrix composition has a direct effect on the neutron, sonic, and density logs. In our work, we applied the binary and tri-porosity cross-plots of the Rudeis and Kareem reservoir data in the R-5A well using logs data and Schlumberger charts (Schlumberger 2009). The relation between density-neutron logs is affected by sandstone, dolomite, and limestone as reservoirs when

they cross-plotted with each other, besides shale and evaporates. All neutron involvement is limestone apparent porosity. Shale impact can be noticed on the cross-plot, where the shale impacts are concentrated in the southeast quadrant of the cross-plot (Poupon and Leveau 1971). The effect of the light hydrocarbons and gas through the zone of investigation make porosity of the density log expand and porosity from the neutron log to decrease, where northwest shifted data from the limestone line but is still parallel to the porosity lines. The neutron-density cross-plots in Rudeis and Kareem formations reflect the existence of limestone, sand, and shale with different proportions.

Figure 10a represents the cross-plot that shows the relationship between neutron and density for the Rudeis Formation, revealing that most of the plotted points are concentrated around the limestone reflecting a porosity ranging from 7 to 23% and some points are indicating the shale. This may signify the existence of shale and limestone matrix lithologies. There is no influence of gas effect. Figure 10b elucidates limestone facies and points located on shale for the Kareem Formation, with porosity of more than 20%. This may indicate the existence of shale, limestone matrix lithologies (Al Muhaidib et al. 2012). Shale influence can be remarked on the plot, where the shale influences tend to be in the southeast quadrant. The observation of the effect of gas where some points have moved upwards. Salt and anhydrite are represented with zero-porosity points in the southwest quadrant of the cross plot.

Sonic-neutron plots differentiate limestone, quartz, and dolomite. Saleh et al. (2021) represented that the sonic log responds to primary porosity and largely ignores vuggy porosity and fractures; the influence of secondary porosity is shown on the cross-plot. Involving the sonic log, secondary porosity will displace the points from the correct lithology line and indicate something less than the total porosity (Jafri et al. 2016). The sonic-neutron cross-plot in lower Miocene sediments reflects the existence of limestone, shale, and sandstone with different proportions (Fig. 11a, b). The majority of the readings are limestone and some

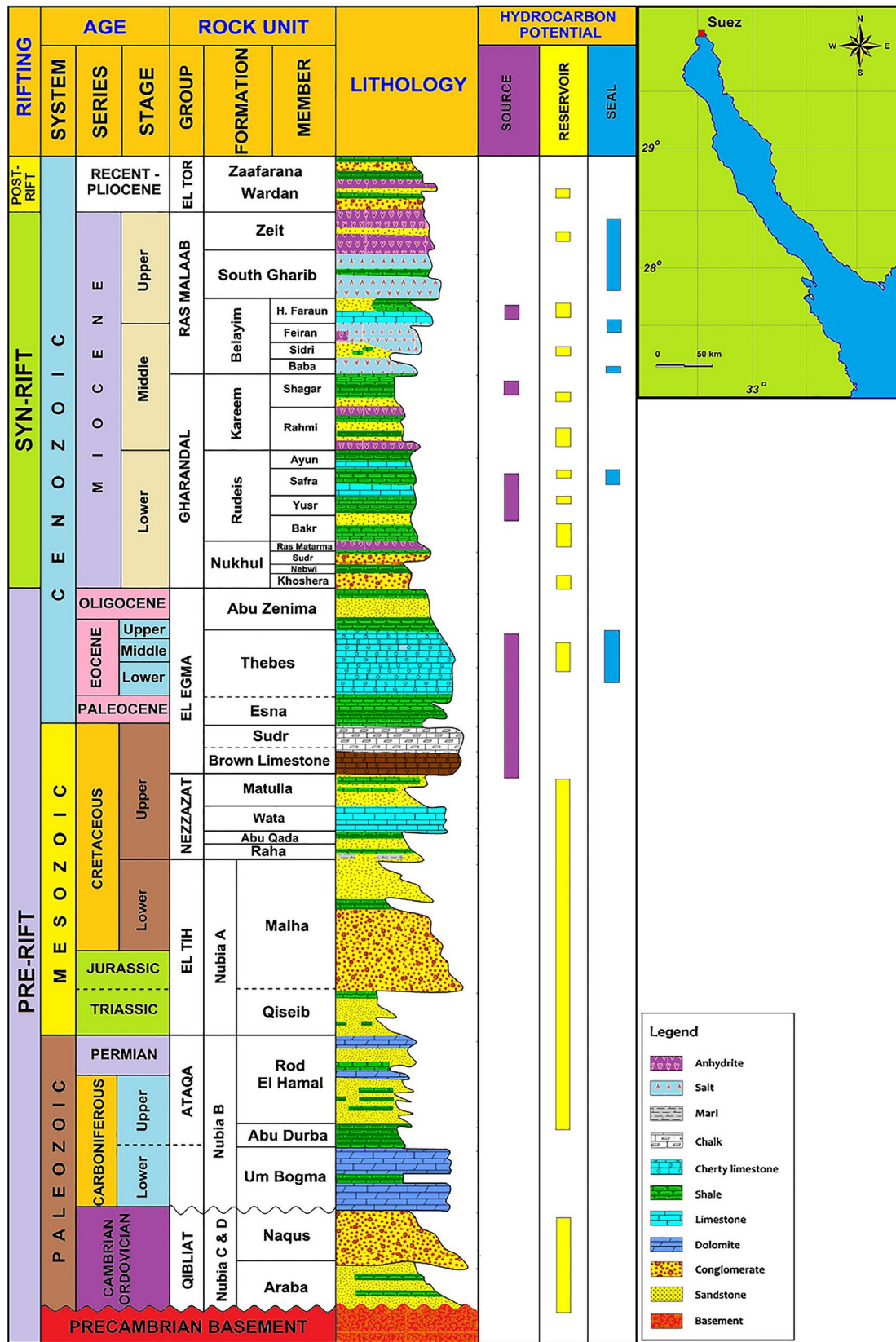
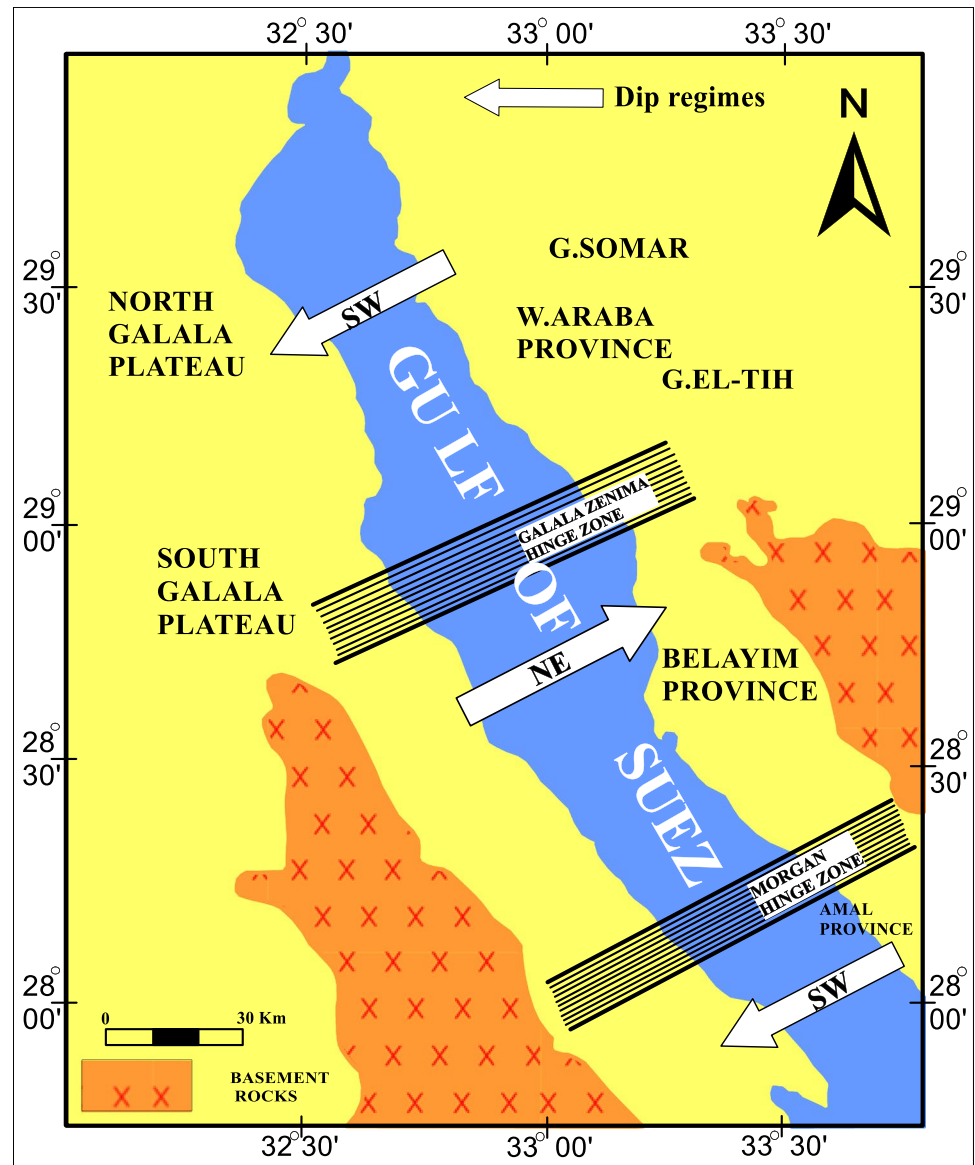


Fig. 2 Generalized stratigraphic column of the central Gulf of Suez (El Diasty et al. 2019)

Fig. 3 Generalized Gulf of Suez massive tectonic provinces (modified after Moustafa, 1976)



points reveal sandstone and shale with the existence of anhydrite. Cross-plots of sonic-density are advantageous for causal evaporite minerals such as anhydrite, gypsum, and salt. Several log data points show it is corresponding to various mixtures of anhydrite, salt, and dolomite. The sonic-density cross-plot implies the existence of shale, anhydrite, and limestone with diverse proportions (Fig. 12a, b). Most points are concentrated around the limestone while some points are presented around sandstone and shale.

The M–N cross-plot is an old but effective technique for determining lithology. The (M–N) cross plot or three-dimensional (3-D) cross-plot often called litho-porosity cross-plot and is used to identify mineral types in the matrix. The three porosity logs readings were combined to yield M and N parameters, which are independent of

porosity. M and N are computed by the following formula: $M = ((\Delta t_f - \Delta t) / (\rho_b - \rho_f)) \times 0.01$, where Δt_f is the transit time of the saturation fluid, ρ_b is the density log reading, and ρ_f is the fluid density; $N = (\Phi N_f - \Phi N) / (\rho_b - \rho_f)$, where ΦN_f is the hydrogen index of the fluid and ΦN the neutron log reading. For saline mud, $\Delta t_f = 184 \mu\text{s}/\text{ft}$, $\rho_f = 1.1 \text{ gm}/\text{cc}$ and $\Phi N_f = 100\%$ (Burke et al. 1969). Figure 13a and b show the mineralogical composition of the Rudeis and Kareem reservoirs. Utmost the points fill in between calcite, quartz, and anhydrite. This may indicate the presence of mixed lithologies. The Kareem Formation is syn-rifting sediments that reflect fluctuating of some readings up signifying, a secondary porosity manifestation. The last distorted points are strewn and shifted downwards as a result of the shale effects. Also,

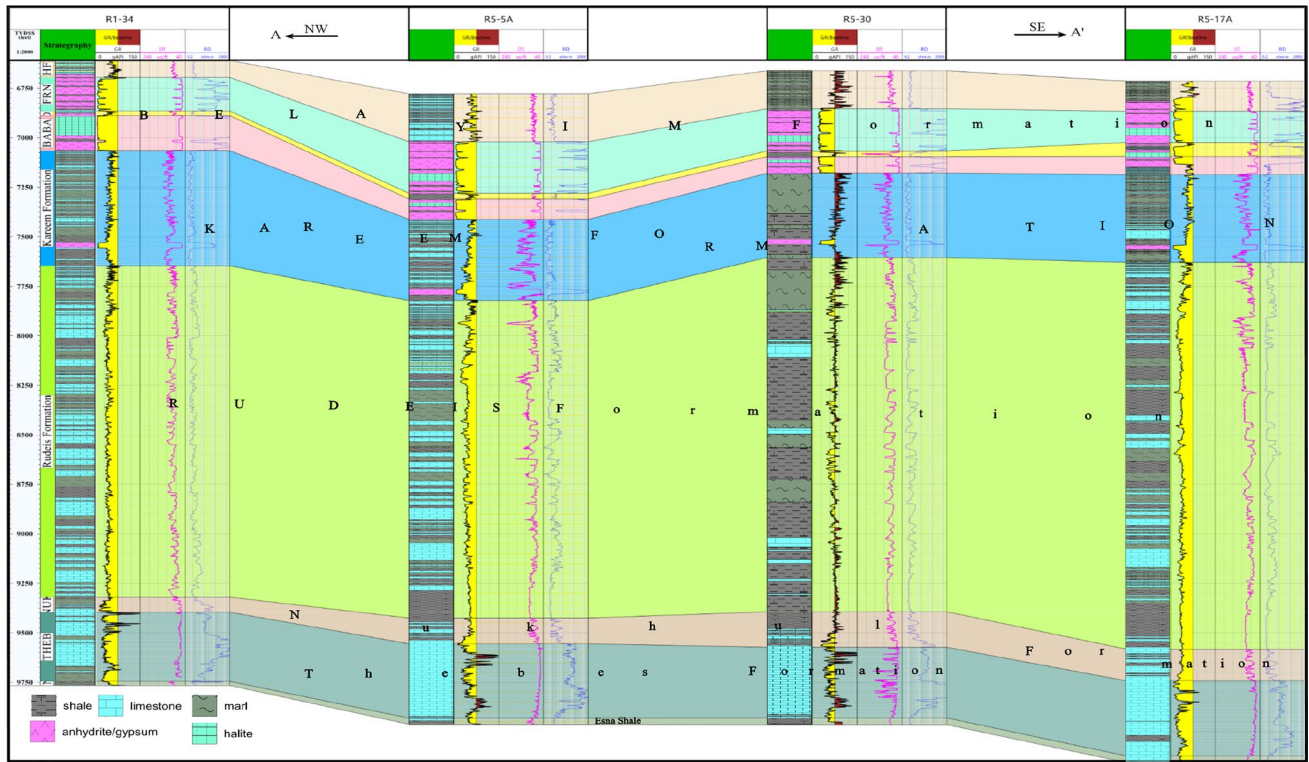


Fig. 4 Lithostratigraphic correlation cross section of the Miocene succession of Ramadan oil field using electric logs

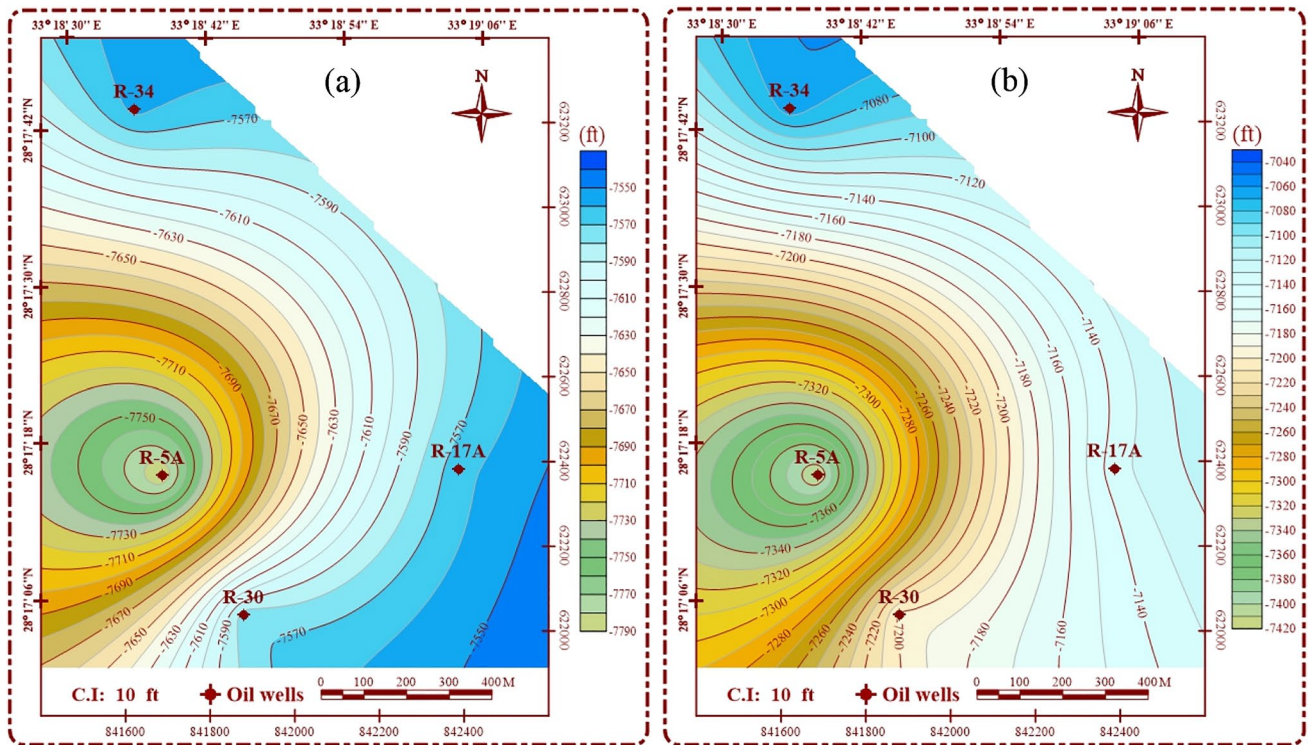


Fig. 5 Relief maps of a Rudeis Formation and b Kareem Formation

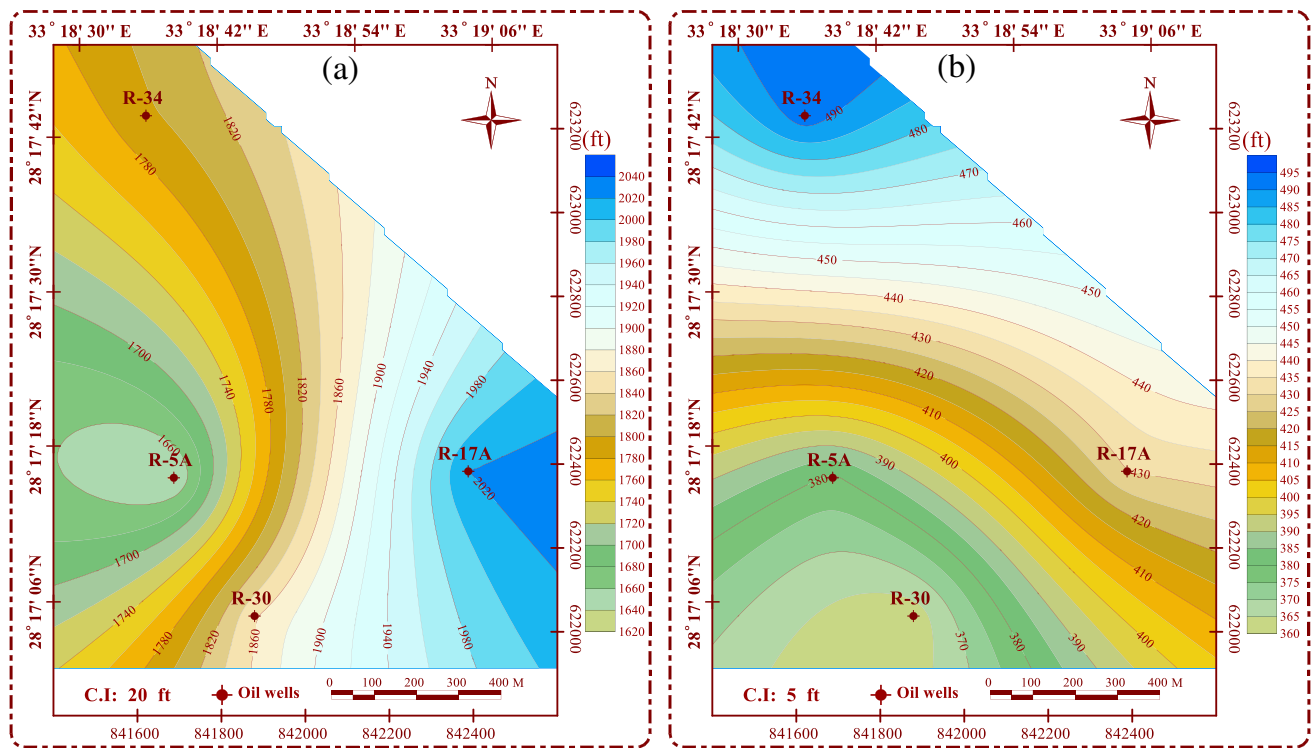


Fig. 6 Isopach maps of **a** Rudeis Formation and **b** Kareem Formation

the influence of gas shows in shifting a few points to the upright corner of the diagram.

Source rock characteristics

TOC results for the Rudeis and Kareem formations in the WFB-1 and GS197-2 wells vary from poor to good organic content. The Rudeis Formation reflected a poor to good organic matter potential where the TOC content ranged from 0.33 to 1.21 wt.% in the WFB-1 well and 0.42 to 1.23 wt.% in the GS197-2 well (Fig. 14a, b). The Kareem Formation also reflected the same rating in the WFB-1 well, with TOC content ranging from 0.44 to 1.19 wt. % (Fig. 14a). According to Peters and Cassa (1994), Rock–Eval pyrolysis data results of S_1 values reflected that the Rudeis Formation samples at the WFB-1 and GS197-2 wells have free hydrocarbon S_1 values ranging from 0.13 to 0.35 mg/g and 0.15 to 0.41 mg/g, respectively. It shows indigenous hydrocarbon present (Fig. 15a, b). The Kareem Formation in the WFB-1 well has S_1 values ranging from 0.16 to 0.35 mg/g, which reflect indigenous hydrocarbon presence (Fig. 15a). The presentation of S_2 values for Rudeis Formation at the WFB-1 and GS197-2 wells is shown in Fig. 16a, b where the S_2 values range from 0.07 to 3.16 mg/g and 0.56 to 3.2 mg/g, respectively. It shows type III gas-prone and mixed type II/III oil–gas-prone. The S_2 values of the Kareem Formation in well WFB-1 range from 0.77 to 3.74 mg/g, which reflects

a mixed type II/III oil–gas prone, and type III gas-prone (Fig. 16a). Hunt (1996) ranked hydrocarbon quality index as (QI) between 2 and 5 for oil/gas-prone, > 5 for oil-prone, and is < 2 for gas-prone organic matter (Gogoi et al. 2008). The quality index of hydrocarbons (QI) for the Rudeis Formation ranged from 0.2 to 3.1 in the WFB-1 well and from 0.2 to 1.6 in the GS197-2 well, respectively (Fig. 17a, b), indicating mainly gas-prone organic matter. The QI for the Kareem Formation fluctuates from 0.7 to 2.3, which indicates mainly gas (Fig. 17a).

The HI and OI values for Rudeis Formation at the WFB-1 well range from 19 to 762 mg HC/g TOC and 58 to 495 mg HC/g CO_2 , respectively. It ranges from 169 to 757 mg HC/g TOC and 114 to 303 mg HC/g CO_2 , respectively, at the GS197-2 well, indicating type III gas-prone and mixed type II/III kerogen (Fig. 18a, b). For the Kareem Formation at WFB-1 well, the HI and OI values range from 148 to 343 mg HC/g TOC and 117 to 325 mg HC/g CO_2 , respectively (Fig. 18a). This denotes a potential source rock for generating type III and mixed type II/III kerogen (Jackson et al. 1985). The relationship between TOC % and HI for Rudeis and Kareem formations at the WFB-1 wells indicates that the oil potential of these formations is a fair source rock (Fig. 19a). The relationship between TOC % and HI for the Rudeis Formation at the GS197-2 well (Fig. 19b) indicates that gas and / or oil source and gas pron. The pyrolysis T_{max} values of

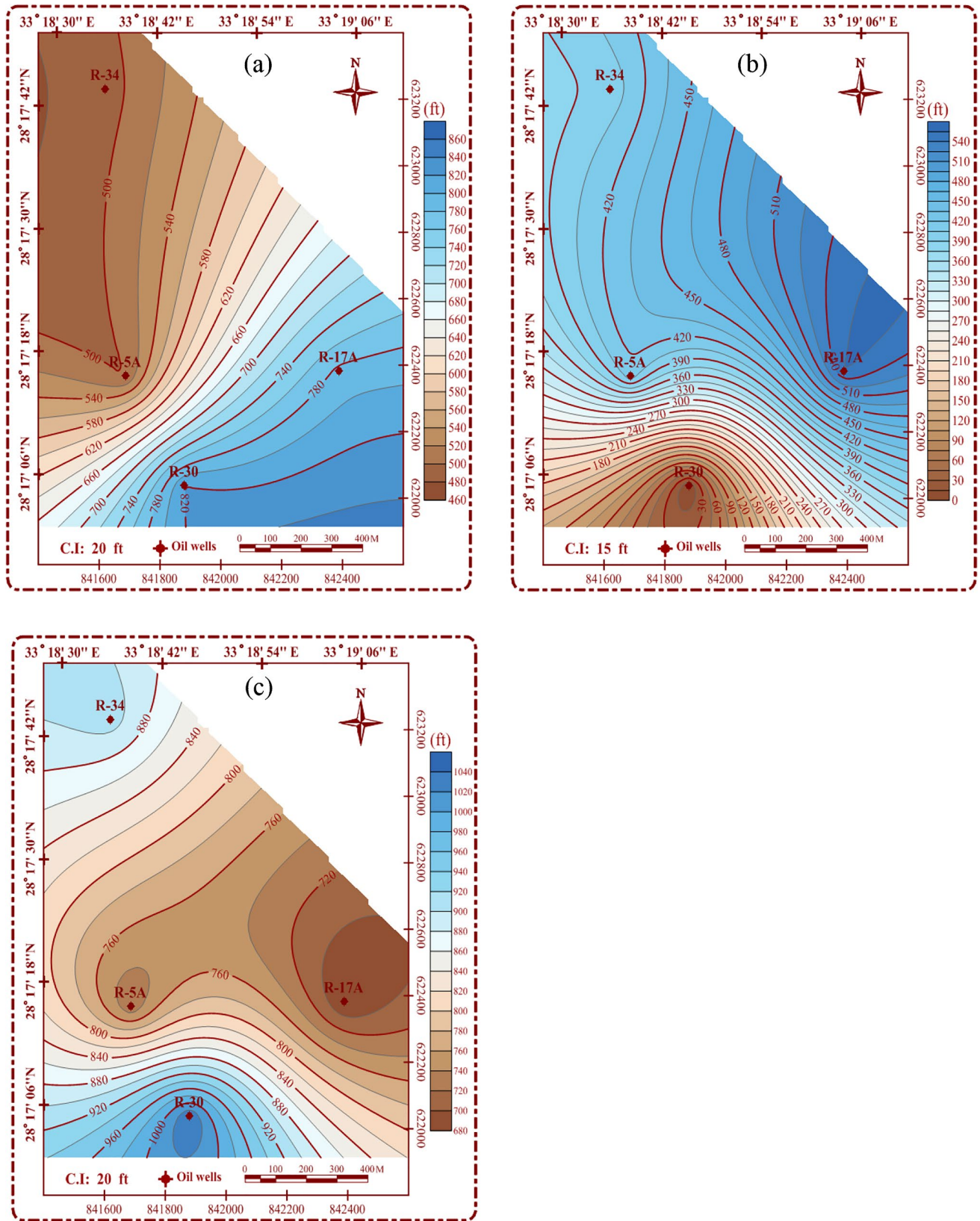


Fig. 7 Isolith maps of Rudeis Formation. a Shale isolith. b Marl isolith. c Limestone isolith

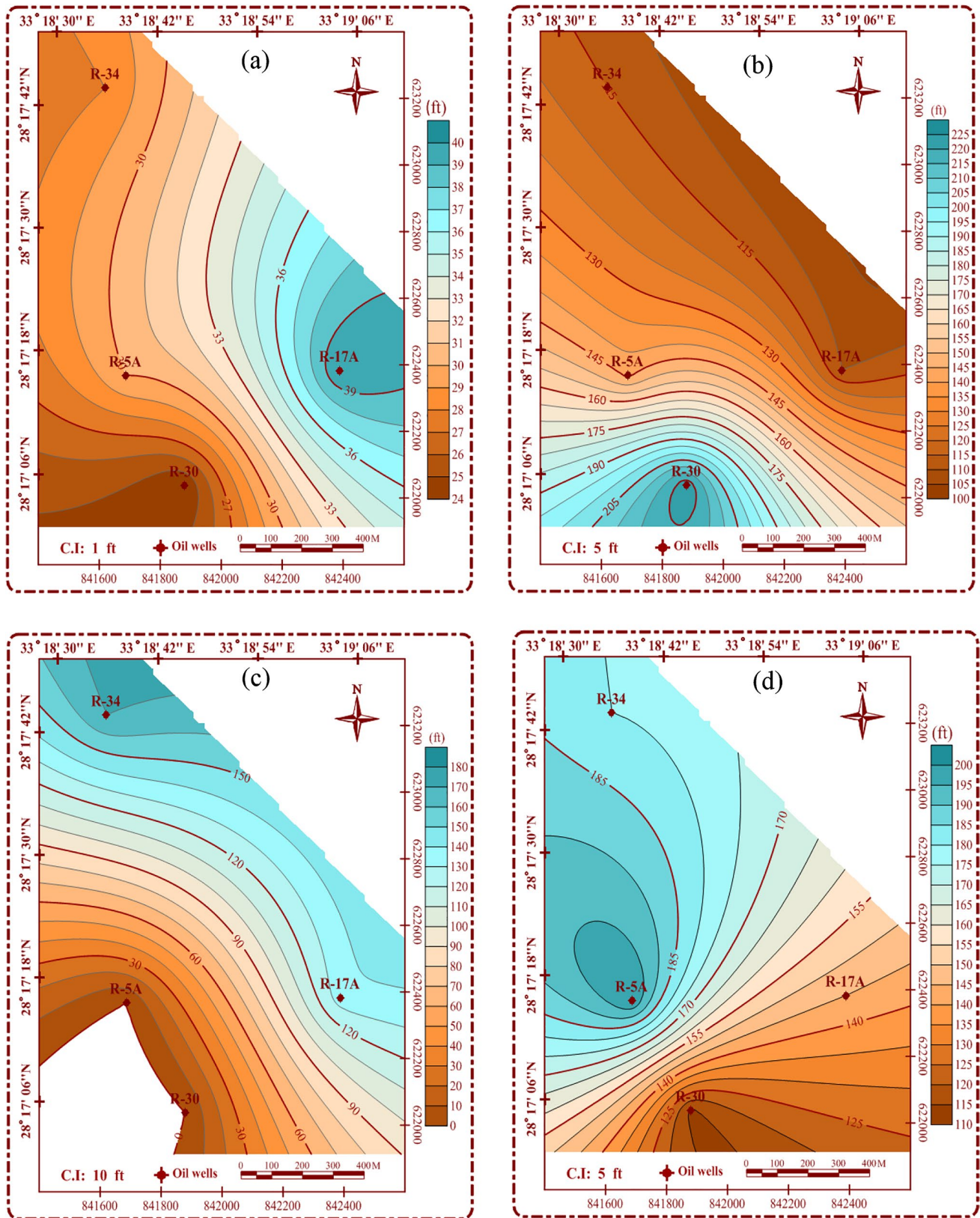


Fig. 8 Isoloth maps of Kareem Formation. **a** Anhydrite isoloth. **b** Limestone isoloth. **c** Marl isoloth. **d** Shale isoloth

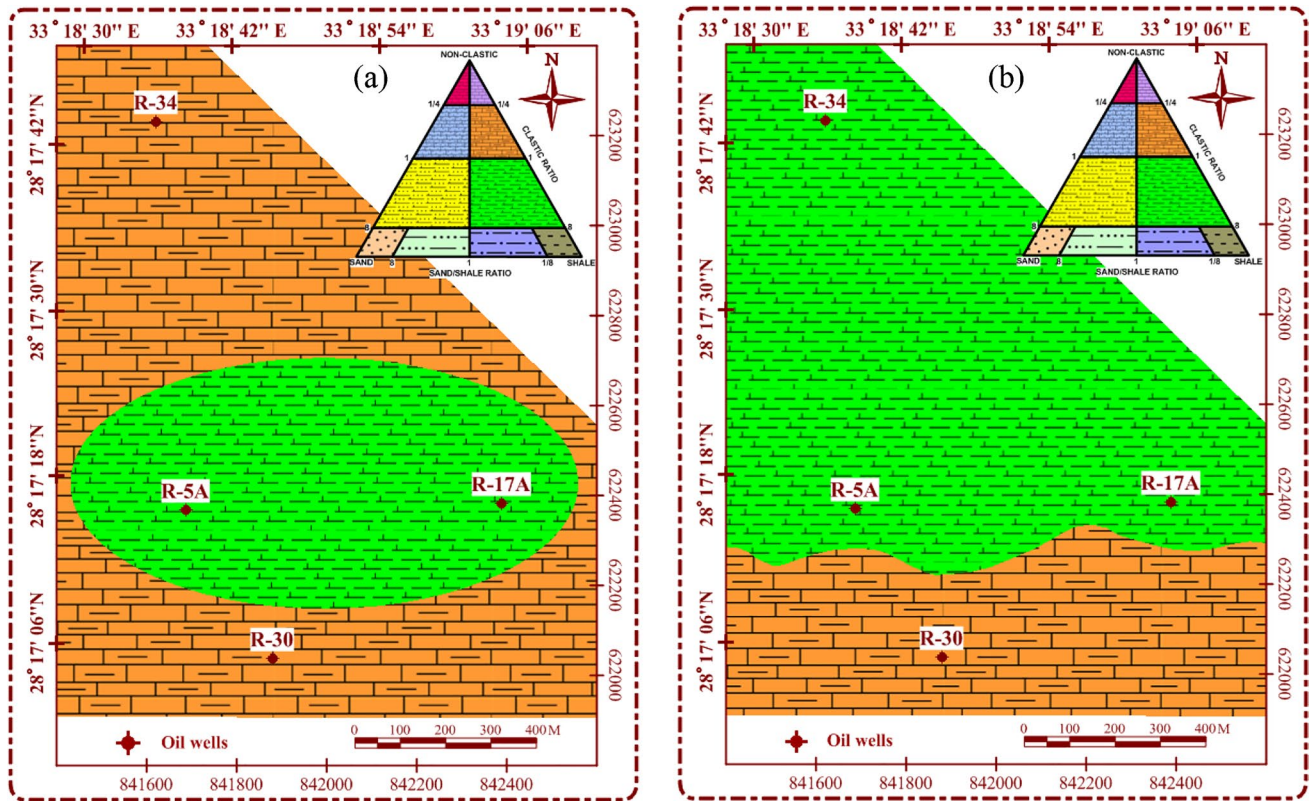


Fig. 9 Lithofacies maps of **a** Rudeis Formation and **b** Kareem Formation

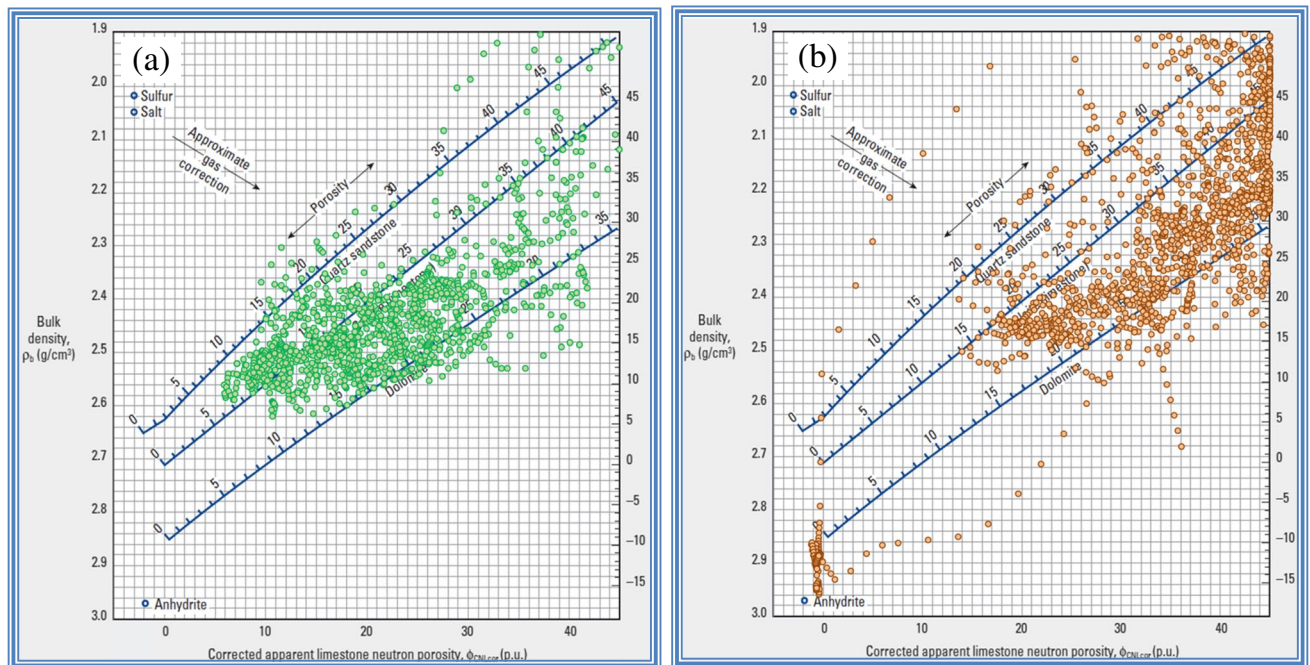


Fig. 10 Neutron–density cross-plot of **a** Rudeis Formation and **b** Kareem Formation in R-5A well

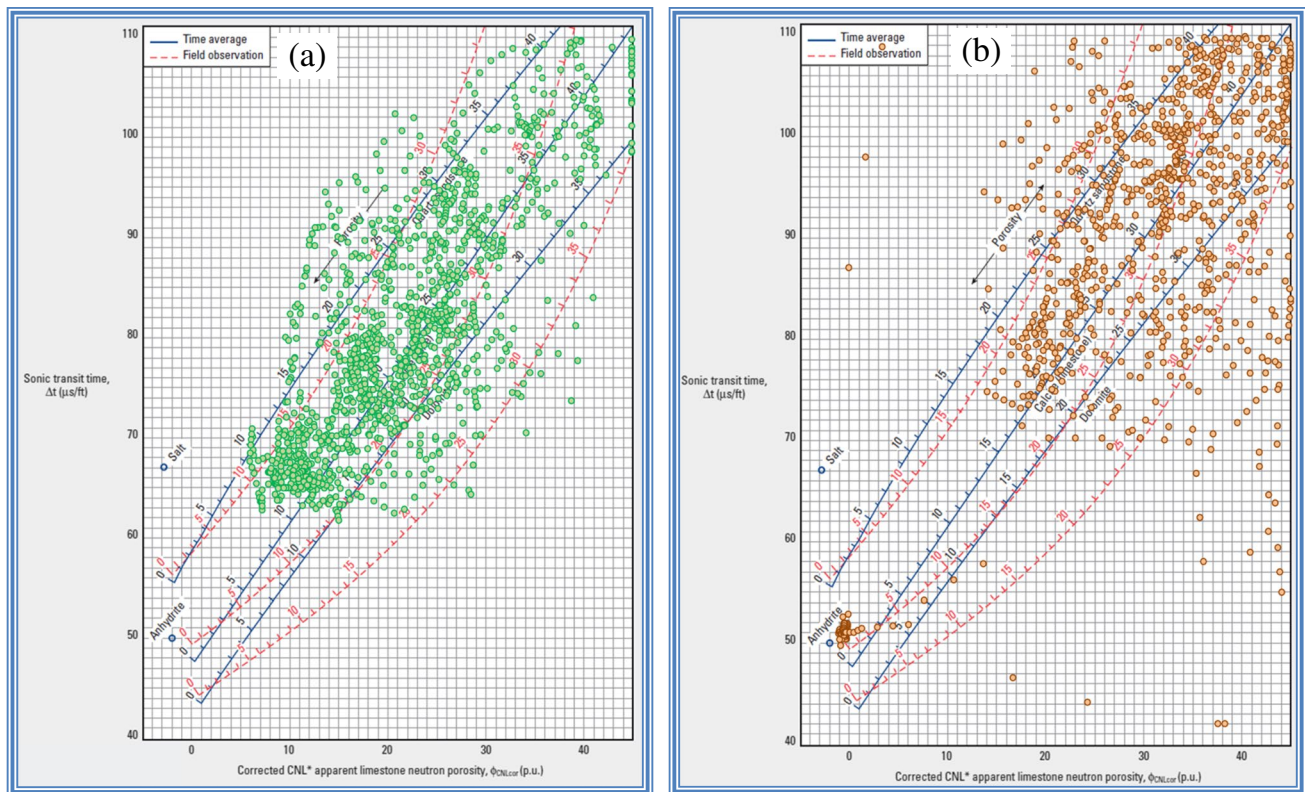


Fig. 11 Neutron–sonic cross-plot of **a** Rudeis Formation and **b** Kareem formation in R-5A well

the investigated samples in the Rudeis Formation at the WFB-1 and GS197-2 wells range from 421 to 433 °C and 419 to 435 °C; respectively. This indicates that the investigated source rocks are (immature biogenic and immature oil) mixed type II/III and type III (Fig. 20a, b). Figure 20a shows the T_{max} values of Kareem Formation which, range from 421 to 432 °C reflecting immature biogenic and immature oil mixed type II/III and type III (Carvajal-Ortiz and Gentzis 2015).

Kerogen's thermal maturity is predominantly based on the vitrinite reflectance (R_o %), T_{max} values, and PI. The PI of the Rudeis Formation at the WFB-1 and GS197-2 wells ranges from 0.1 to 0.7 and 0.1 to 0.3, respectively. It fluctuates from 0 to 0.2 for Kareem Formation at WFB-1 well, as the relationship between the PI and T_{max} reveals an immature to marginally mature source rock (Fig. 21a, b). Figure 22a and b show the relationship between the calculated R_o and HI for the Kareem and Rudeis formations at the WFB-1 and GS197-2 wells which indicates mixed type II/III and type III gas-prone source rocks. Tables 2, 3, and 4 reflect that the generation potential of the Rudeis and Kareem formations (GP) ranges from 0.2 to 3.4 mg HC/g and 0.8 to 3.6 mg HC/g rock, respectively. These

data reveal that the organic richness of these formations fluctuates from non-source to poor generation potential. The generation potential of the Kareem Formation fluctuates from 1.0 to 3.9 mg HC/g rock. These data expose that the organic richness of the Kareem Formation varies from poor to moderate GP.

Conclusions

The stratigraphic chart reflects a deeper sedimentation water in the southern parts for the Rudeis Formation and lagoonal lower part of Kareem formation reflecting a shallow environment due to the major regional marine regression along the Gulf of Suez that resulted in the deposition of a thin anhydrite layer at the Rahmi member. The Kareem formation has more shale southward the same as the Rudeis Formation. The relief maps of the Rudeis and the Kareem formations show an increased depth in the western parts, which, reflect a suitable environment for oil maturation, and generation in these parts of the investigated area. This reflects a sedimentary basin with a western depocenter and northern, northwestern, and western low dip gradient

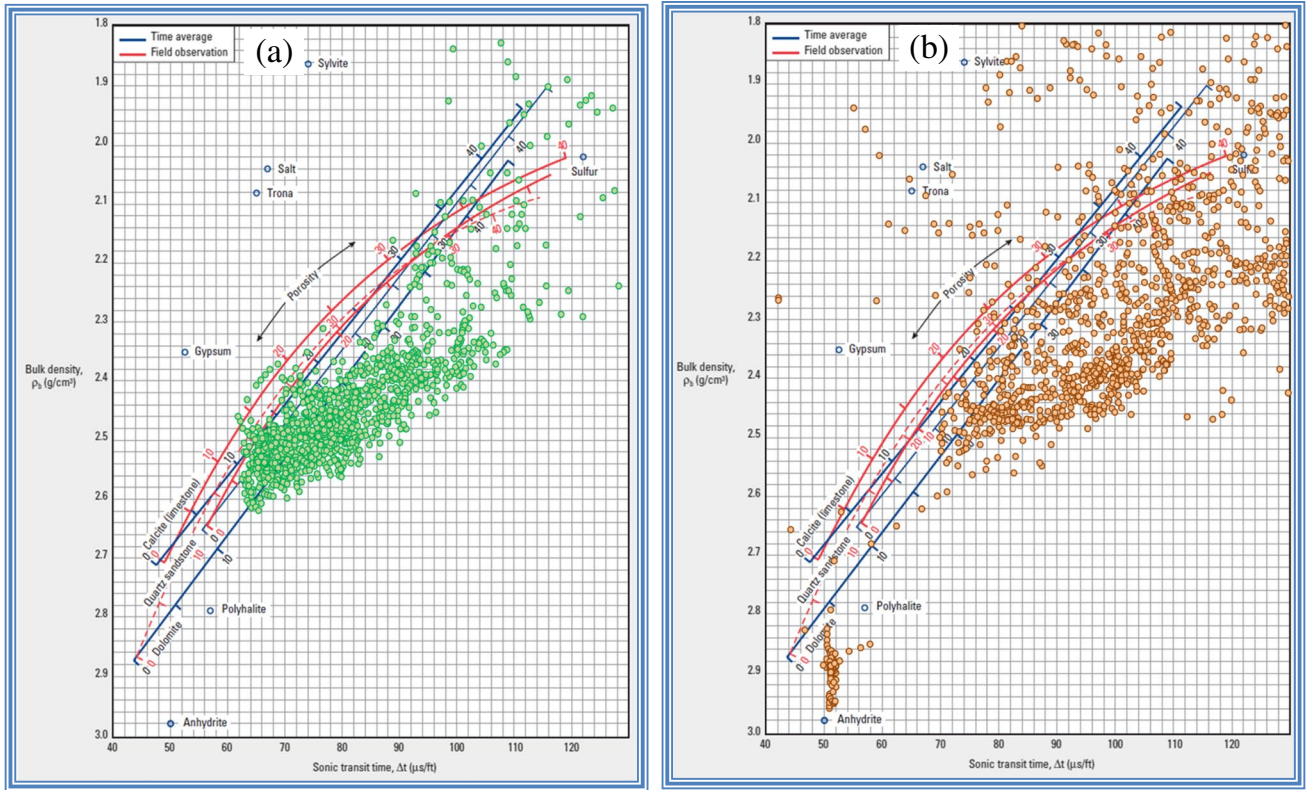


Fig. 12 Sonic–density cross-plot of **a** Rudeis Formation and **b** Kareem Formation in R-5A well

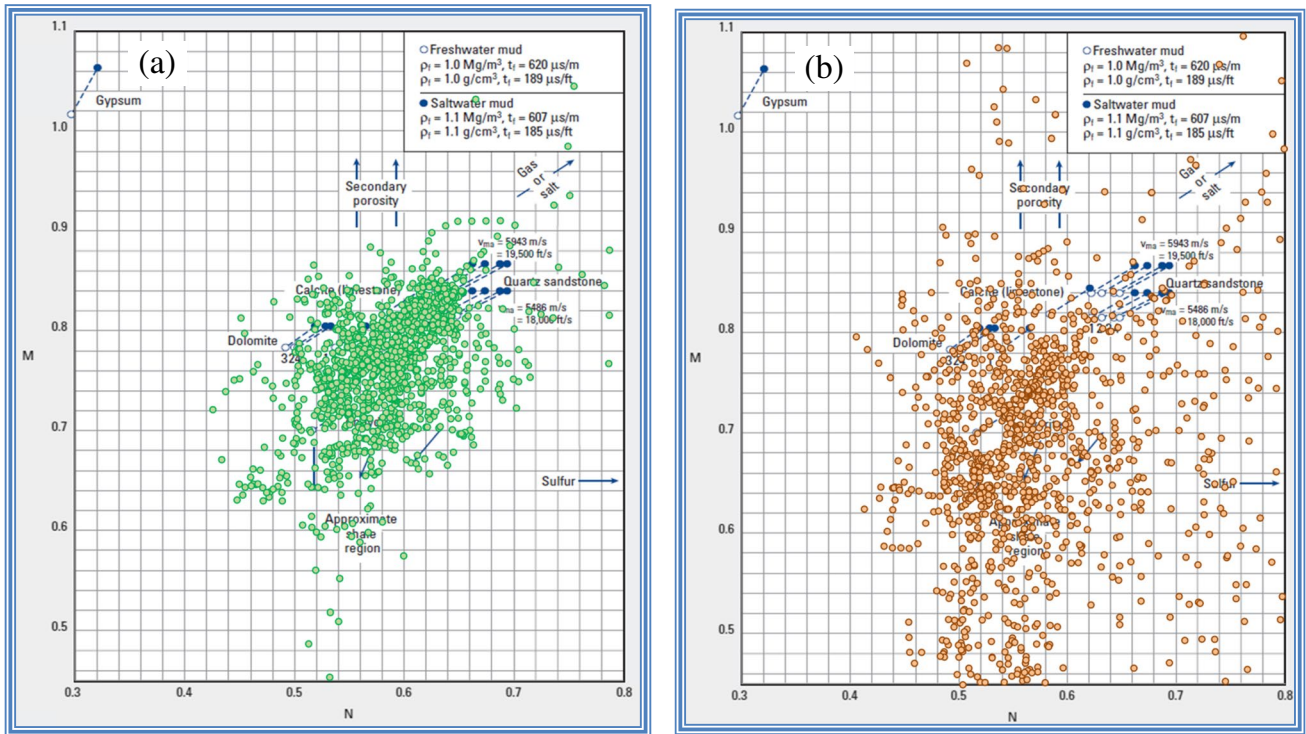


Fig. 13 M–N cross-plot of **a** Rudeis Formation and **b** Kareem Formation in R-5A well

Fig. 14 Cross-plot of variations of TOC content with depth in **a** Rudeis and Kareem formations in WFB-1 well and **b** Rudeis Formation in GS197-2 well, Central Gulf of Suez, Egypt

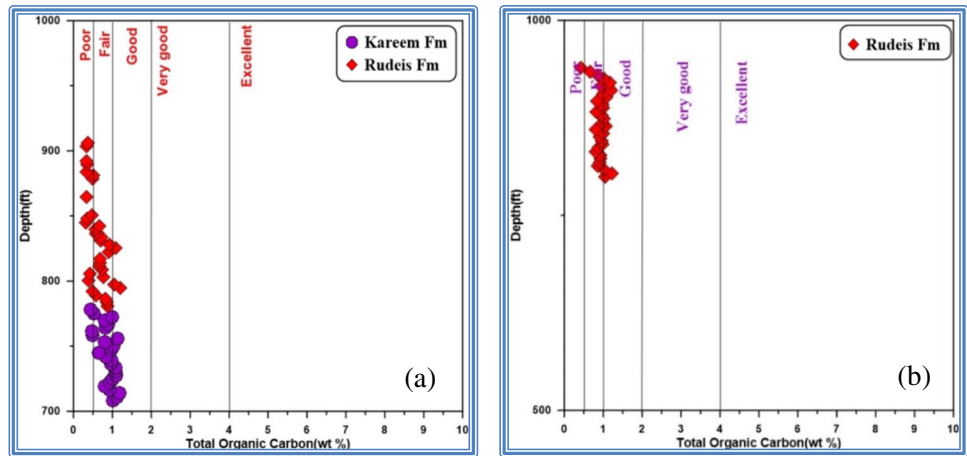


Fig. 15 Cross-plot of Rock-Eval S_1 versus TOC (wt %) of **a** Kareem and Rudeis formations in WFB-1 well and **b** Rudeis Formation in GS197-2 well, Central Gulf of Suez, Egypt

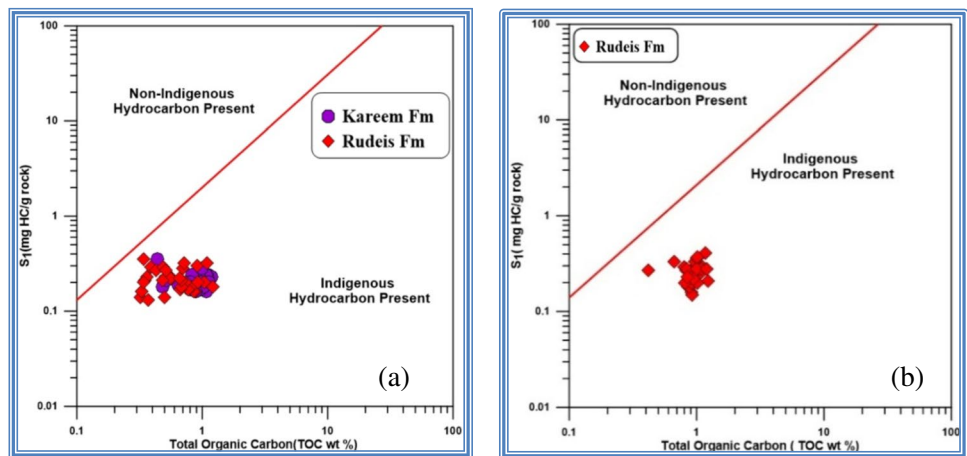
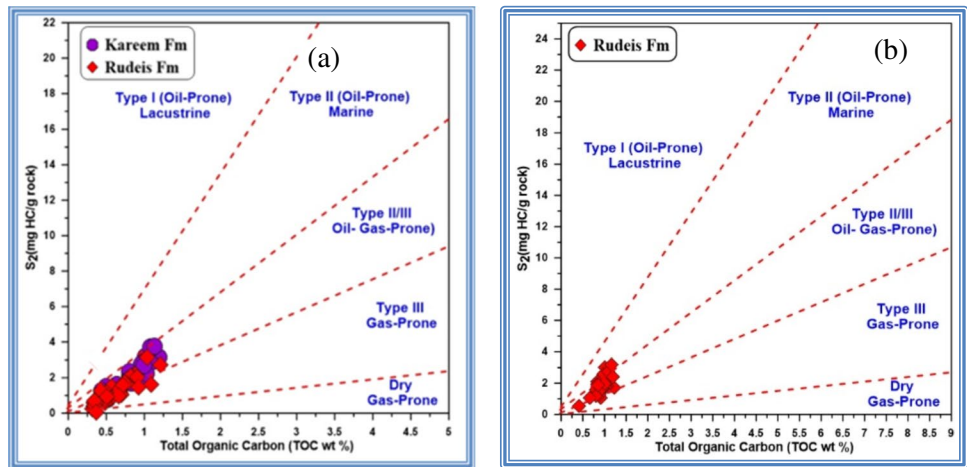


Fig. 16 Cross-plot of Rock-Eval S_2 versus TOC (wt %) of **a** Kareem and Rudeis formations in WFB-1 well and **b** Rudeis Formation in GS197-2 well, Central Gulf of Suez, Egypt



platform margin for the Rudeis formation, which inverted slightly into a high dip gradient for the Kareem Formation. The Rudeis Formation thickness increases towards the east and decreases towards the west. The thickness of the Kareem Formation expands towards the north, while

it diminishes towards the southern parts of the investigation area.

Lithofacies map shows that the sediments consist of shaley limestone and calcareous shale facies, indicating a shallow to deep marine depositional environment.

Fig. 17 Cross-plot of quality index (S_2/S_3) versus depth for **a** Kareem and Rudeis formations in WFB-1 well and **b** Rudeis Formation in GS197-2 well, Central Gulf of Suez, Egypt

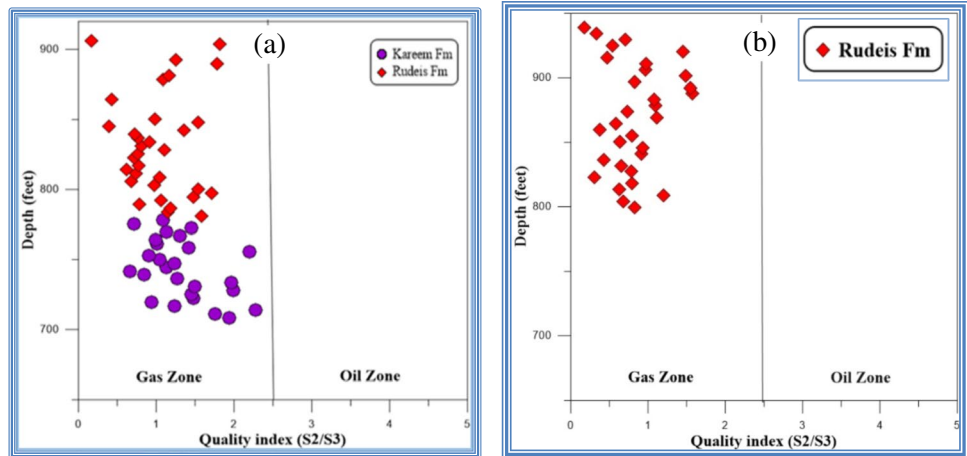


Fig. 18 Cross-plot of OI versus HI (Espitalié et al. 1985) for different kerogen types in **a** Kareem and Rudeis formations in WFB-1 well and **b** Rudeis Formation in GS197-2 well, Central Gulf of Suez, Egypt

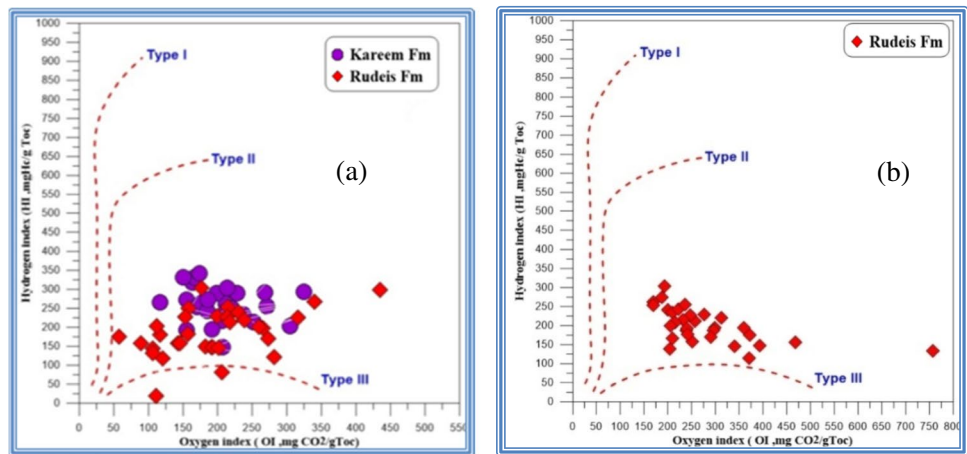
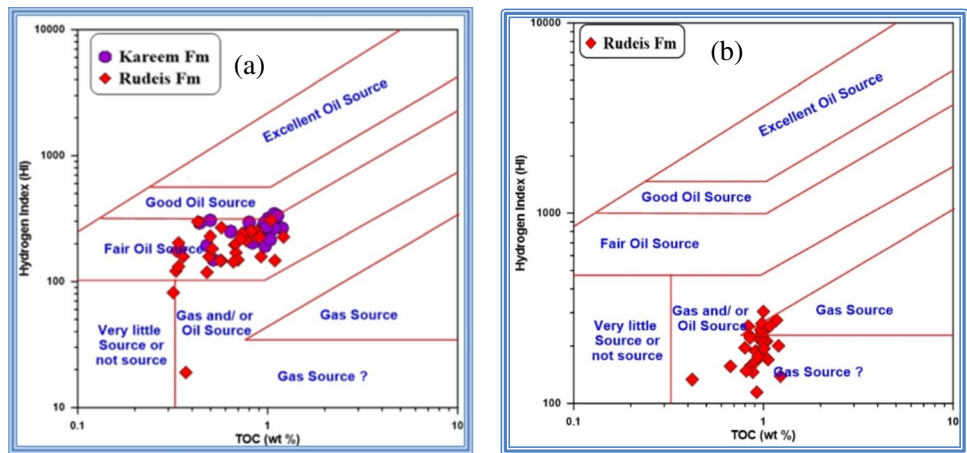


Fig. 19 Source rock characterization based on HI and TOC (Jackson et al. 1985) for **a** Kareem and Rudeis formations in WFB-1 well and **b** Rudeis Formation in GS197-2 well, Central Gulf of Suez, Egypt



The binary porosity cross plot and tri-porosity cross plot (M–N) of Rudeis and Kareem reservoir data in R-5A well indicate the presence of limestone, shale, sand, and anhydrite with different proportions with porosity fluctuating from 7 to 25%. The Kareem Formation is immature

and has a non-source to poor generating capability for both oil and gas. The Rudeis Formation in the WFB-1 and GS197-2 wells is immature with few samples that are mature having non-source to poor generating capability for both oil and gas. The Kareem Formation in the WFB-1

Fig. 20 Plot of HI versus T_{max} for **a** Rudeis and Kareem formations in WFB-1 well and **b** Rudeis Formation in GS197-2 well

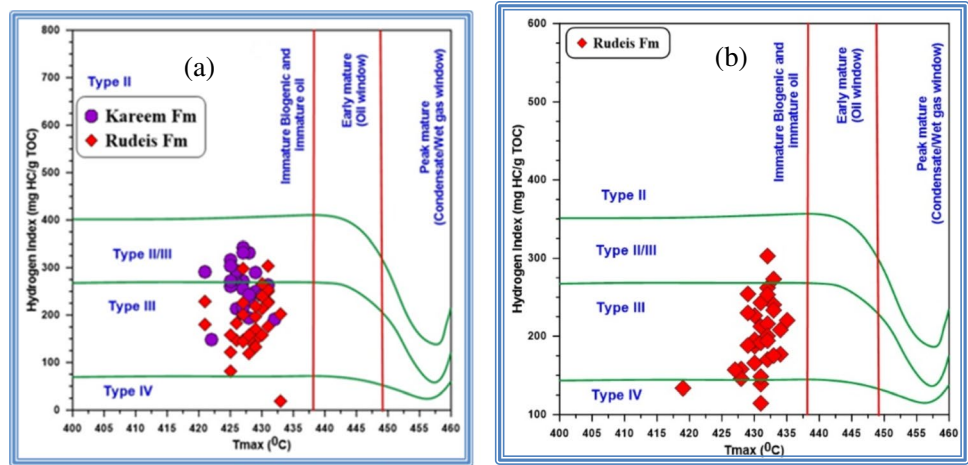


Fig. 21 Cross-plot of T_{max} versus PI for **a** Kareem and Rudeis formations in WFB-1 well and **b** Rudeis Formation in GS197-2 well, Central Gulf of Suez, Egypt

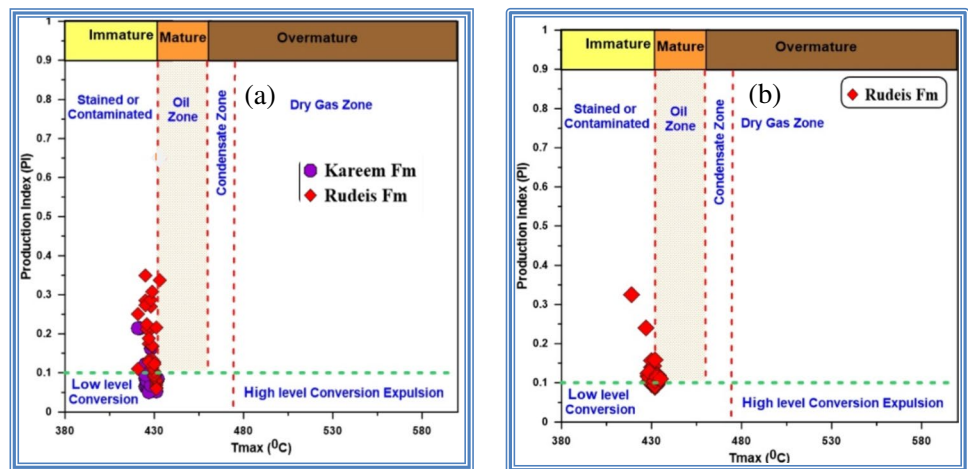
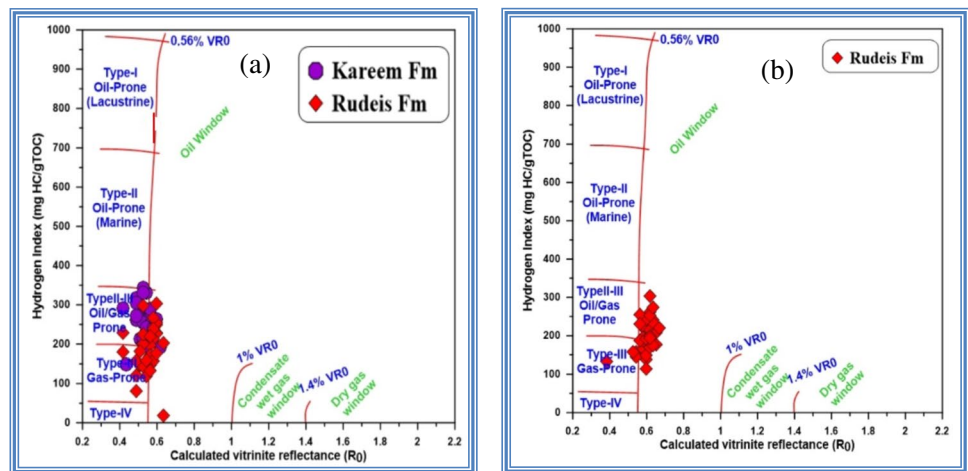


Fig. 22 HI versus calculated R_o of Hunt (1996) for **a** Kareem and Rudeis formations in WFB-1 well and **b** Rudeis Formation in GS197-2 well, Central Gulf of Suez, Egypt



well is immature to marginally mature source rock, which has non-source to poor generating capability for both oil and gas. It lies within the early generation window of oil. The subsurface and source rock characterization results of the investigated succession reflected that the lower

Miocene sediments north of the Ramadan oil field are non-source to poor source rocks.

Acknowledgements The authors appreciate the Gulf of Suez Petroleum Company and the Egyptian General Petroleum Corporation for

providing the data. The same as the reviewers and the Editor of the Journal of Arabian Geosciences Science for their appreciated clarifications, which upgraded the novelty of the manuscript.

Funding Open access funding provided by The Science, Technology & Innovation Funding Authority (STDF) in cooperation with The Egyptian Knowledge Bank (EKB).

Declarations

Conflict of interest The authors declare no competing interests.

Open Access This article is licensed under a Creative Commons Attribution 4.0 International License, which permits use, sharing, adaptation, distribution and reproduction in any medium or format, as long as you give appropriate credit to the original author(s) and the source, provide a link to the Creative Commons licence, and indicate if changes were made. The images or other third party material in this article are included in the article's Creative Commons licence, unless indicated otherwise in a credit line to the material. If material is not included in the article's Creative Commons licence and your intended use is not permitted by statutory regulation or exceeds the permitted use, you will need to obtain permission directly from the copyright holder. To view a copy of this licence, visit <http://creativecommons.org/licenses/by/4.0/>.

References

- Al Muhaidib AM, Sen MK, Toksoz MN (2012) Integration of geology, rock physics, logs, and prestack seismic data for reservoir porosity estimation. *AAPG Bull* 96(7):1235–1251
- Behar F, Beaumont V, Penteado HL, De B (2001) Rock-Eval 6 technology: performances and developments. *Oil Gas Sci. Technol Rev Inst Fr Pet Energy* 56:111–134
- Burke JA, Campbell RLJ, Schmidt AW (1969) The litho porosity cross plot: a new concept for determining porosity and lithology from logging methods. Paper presented at the SPWLA 10th Ann. Logging Symp. No. 6., Houston, Texas.
- Carvajal-Ortiz H, Gentzis T (2015) Critical considerations when assessing hydrocarbon plays using Rock-Eval pyrolysis and organic petrology data: *Int. J Coal Geol* 152:113–122
- Dott RHJ (1964) Wacke, graywacke and matrix: approach to immature sandstone classification. *J Sediment Res* 34(3):625–632
- Egyptian General Petroleum Corporation (EGPC) (1964) Oligocene and Miocene rock stratigraphy of the Gulf of Suez region. In: Ghorab, M.A., et al. (Eds.), EGPC, Consultative Stratigraphic Committee, Cairo, Egypt, 142 p
- El Diasty WS, Abo Ghonaim AA, Mostafa AR, El Beialy SY (2014) Biomarker characteristics of the Senonian-Eocene succession, Belayim oilfields, central Gulf of Suez. *Egypt Mansoura J Environ Sci* 43:407–429
- El Diasty W S, El Beialy S Y, Mostafa A R, Abo Ghonaim A A, Peters K E (2019) Chemometric differentiation of oil families and their potential source rocks in the Gulf of Suez. *Nat Resour Re* 29:2063–2102. <https://doi.org/10.1007/s11053-019-09569-3>
- El Diasty W S, Peters K E (2014) Genetic classification of oil families in the central and southern sectors of the Gulf of Suez, Egypt. *J Pet Geol* 37:105–126. <https://doi.org/10.1111/jpg.12573>
- El Khadragey AA, AbdElrazik EED, Azam SS, Saleh AH (2016) Integrated petrophysical and lithofacies studies of lower-middle Miocene reservoirs in Belayim marine oil field, Gulf of Suez. *Egypt J Earth Sci* 117:331–344
- El Shazly S, Garossino GA (1991) Ramadan oil field Annual Meeting of American Association of Petroleum Geologists, United States. *AAPG Bulletin* 75:3
- El-Ghali MAK, El Khoriby E, Mansurbeg H, Morad S, Ogle N (2013) Distribution of carbonate cements within depositional facies and sequence stratigraphic framework of shoreface and deltaic arenites, Lower Miocene, the Gulf of Suez rift. *Egypt Mar Petrol Geol* 45:267–280. <https://doi.org/10.1016/j.marpetgeo.2013.04.019>
- Espitalié J, Deroo G, Marquis F (1985) Rock-Eval pyrolysis and its application. *Inst. Fr. Preprint* 33578, 72 p
- Espitalié J, Laporte J L, Madec M, Marquis F, Leplat P, Paulet J, Boutefeu A (1977) Methode rapid de caracterisation des roches. Mere de leur potential petrolier of de leur degre evolution. *Rev. de I. Inst France Petrol* 32(1): 32–42
- Gogoi K, Dutta MN, Das PK (2008) Source rock potential for hydrocarbon generation of Makum coals, Upper Assam. *India Curr Sci* 95:233–239
- Hadad YT, Hakimi MH, Abdullah AH, Kinawy M, El Mahdy O, Lashin A (2021) Organic geochemical characteristics of Zeit source rock from Red Sea Basin and their contribution to organic matter enrichment and hydrocarbon generation potential. *J Afr Earth Sci* 177:104–151
- Hughes GW, Abdine S, Girgis MH (1992) Miocene biofacies development and geological history of the Gulf of Suez. *Egypt Mar Pet Geol* 9:2–28
- Hunt JM (1996) Petroleum geochemistry and geology, 2nd edn. W. H. Freeman and Company, New York, p 743
- Jackson KS, Hawkins PJ, Bennett AJR (1985) Regional facies and geochemical evaluation of the southern Denison Trough, Queensland. *APPEA J* 20:143–158
- Jafri MK, Lashin A, Ibrahim E, Naeem M (2016) Petrophysical evaluation of the Tensleep sandstone Formation using well logs and limited core data at Teapot Dome, Powder River Basin, Wyoming, USA. *Arab J Sci Eng* 41:223–247. <https://doi.org/10.1007/s13369-015-1741-7>
- Krumbein WC, Sloss LL (1963) Stratigraphy and sedimentation, 2nd edn. California, Freeman, San Francisco, p 660
- Lashin AA, El-Naby AA (2014) Petrophysical, seismic structural and facies analysis of the Miocene reservoirs of East Morgan oil field, Gulf of Suez. *Egypt Arab J Geosci* 7:3481–3504. <https://doi.org/10.1007/s12517-013-1011-5>
- Makky AF, El Sayed MI, Abd-Allah Z M (2010) hydrocarbon potentiality of some Miocene rock units in the central part of the Gulf of Suez, Egypt. *Int J Acad Res* 2(2):235–248
- Mohamed NS, Shahin AN, El-Kammar AM (2013) Hydrocarbon generating basins and migration pathways in the Gulf of Suez. *Egypt Life Sci J* 10:229–235
- Moustafa A M (1976) Block faulting of the Gulf of Suez. In Proceedings of the 5th Exploration Seminar, unpublished report, Egyptian General Petroleum Corporation, Cairo, pp. 1–19
- Nabawy BS, Mansour AS, Rashed MA, Afify WSM (2019) Implementation of sedimentary facies and diagenesis on the reservoir quality of the Aquitanian-Burdigalian Rudeis Formation in the Gulf of Suez, Egypt: A comparative surface and subsurface study. *Geol J* :1–21. <https://doi.org/10.1002/gj.3683>
- Peters KE, Cassa MR (1994) Applied source rock geochemistry, in Magoon, L.B., and Dow, W.G., Eds., The petroleum system from source to trap. AAPG Memoir 60, pp. 93–120.
- Poupon A, Leveaux J (1971) Evaluation of water saturation in Shaly Formations. Society of Petrophysicists and Well-Log Analysts (SPWLA) 12th Annual Logging Symposium: Dallas Texas 12(4):3–8
- Radwan A (2020) Modeling the depositional environment of the sandstone reservoir in the Middle Miocene Sidri Member, Badri Field, Gulf of Suez Basin, Egypt: integration of gamma-ray log

- patterns and petrographic characteristics of lithology. *Nat Resour Res* 30(1):431–449. <https://doi.org/10.1007/s11053-020-09757-6>
- Radwan A, Sen S (2020) Stress path analysis for characterization of in situ stress state and effect of reservoir depletion on present-day stress magnitudes: reservoir geomechanical modeling in the Gulf of Suez Rift Basin, Egypt. *Natural Resources Research*. <https://doi.org/10.1007/s11053-020-09731-2>
- Saleh AH, Farag AE, Essa EA (2021) Reservoir quality of Abu Roash (G) member in Karama Oil Field, East Bahariya Concession, North Western Desert, Egypt. *Arab J Geosci* 14(169):18P. <https://doi.org/10.1007/s12517-020-06349-9>
- Sallama ES, Afifea MM, Faresb M, van Loonc AJ, Ruban DA (2019) Sedimentary facies and diagenesis of the Lower Miocene Rudeis Formation (southwestern offshore margin of the Gulf of Suez, Egypt) and implications for its reservoir quality. *Mar Geol J* 413:48–70. <https://doi.org/10.1016/j.margeo.2019.04.004>
- Schlumberger (2009) log interpretation chart. 225 Schlumberger Drive, Sugar Land, Texas 77478, pp. 200–260
- Schutz K (1994) Structure and Stratigraphy of the Gulf of Suez, Egypt, in interior Rift Basins. (Ed. S.M. London). *Am Assoc of Petrol Memoir* 59:57–95
- Shazly TF, Ramadan M, El-Sawy MZ (2013) Application of well logs analysis to identify the source rock capabilities of Rudeis and Kareem formations in Rudeis Field, Gulf of Suez. *Egypt J Appl Sci Res* 9(9):5419–5435
- Van Dijk J, Ajayi A T, De Vincenzi L, Ellen H, Guney H, Holloway P, Khdhaouria M, Mcleod I S (2020) Hydrocarbon exploration and production potential of the Gulf of Suez basin. The Framework of the New Tectonostratigraphic Model. *Int. Pet. Tech. Conf., Dhahran, Saudi Arabia*, 13–15 January
- Waples D W (1985) *Geochemistry in Petroleum exploration*. Boston, International Human Resources and Development Corporation pp 232. <https://doi.org/10.1007/978-94-009-5436-6>